Hubble Space Telescope Snapshot Survey for Resolved Companions of Galactic Cepheids: Final Results[*][†]

Nancy Remage Evans[1] , H. Moritz Günther[2] , Howard E. Bond[3,4] , Gail H. Schaefer[5] , Brian D. Mason[6] ,
Margarita Karovska[1] , Evan Tingle[1] , Scott Wolk[1] , Scott Engle[7] , Edward Guinan[7] , Ignazio Pillitteri[8] ,
Charles Proffitt[4] , Pierre Kervella[9] , Alexandre Gallenne[10,11,12] , Richard I. Anderson[13] , and Maxwell Moe[14]

[1] Smithsonian Astrophysical Observatory, MS 4, 60 Garden Street, Cambridge, MA 02138, USA; nevans@cfa.harvard.edu
[2] Massachusetts Institute of Technology, Kavli Institute for Astrophysics and Space Research, 77 Massachusetts Avenue, NE83-569, Cambridge, MA 02139, USA
[3] Department of Astronomy and Astrophysics, Pennsylvania State University, University Park, PA 16802, USA
[4] Space Telescope Science Institute, 3700 San Martin Drive, Baltimore, MD 21218, USA
[5] The CHARA Array, Georgia State University, P.O. Box 3965, Atlanta GA 30302-3965, USA
[6] US Naval Observatory, 3450 Massachusetts Avenue, NW, Washington, DC 20392-5420, USA
[7] Department of Astronomy and Astrophysics, Villanova University, 800 Lancaster Avenue, Villanova, PA 19085, USA
[8] INAF-Osservatorio di Palermo, Piazza del Parlamento 1, I-90134 Palermo, Italy
[9] LESIA, Observatoire de Paris, Université PSL, CNRS, Sorbonne Université, Université de Paris, 5 Place Jules Janssen, F-92195 Meudon, France
[10] Nicolaus Copernicus Astronomical Centre, Polish Academy of Sciences, Bartycka 18, 00-716 Warszawa, Poland
[11] Departamento de Astronomia, Universidad de Concepcion, Casilla 160-C, Concepcion, Chile
[12] Unidad Mixta Internacional Franco-Chilena de Astronomia (CNRS UMI 3386), Departamento de Astronomia, Universidad de Chile, Camino El Observatorio
1515, Las Condes, Santiago, Chile
[13] European Southern Observatory, Karl-Schwarzschild-Straße 2, D-85748 Garching, Germany
[14] University of Arizona, Steward Observatory, 933 N. Cherry Avenue, Tucson, AZ 85721, USA

Abstract

Cepheids in multiple systems provide information on the outcome of the formation of massive stars. They can also lead to exotic end-stage objects. This study concludes our survey of 70 galactic Cepheids using the Hubble Space Telescope (HST) Wide Field Camera 3 (WFC3) with images at two wavelengths to identify companions closer than 5″. In the entire WFC3 survey we identify 16 probable companions for 13 Cepheids. The 7 Cepheids having resolved candidate companions within 2″ all have the surprising property of themselves being spectroscopic binaries (as compared with a 29% incidence of spectroscopic binaries in the general Cepheid population). This is a strong suggestion that an inner binary is linked to the scenario of a third companion within a few hundred astronomical units. This characteristic is continued for more widely separated companions. Under a model where the outer companion is formed first, it is unlikely that it can anticipate a subsequent inner binary. Rather, it is more likely that a triple system has undergone dynamical interaction, resulting in one star moving outward to its current location. Chandra and Gaia data as well as radial velocities and HST/STIS and IUE spectra are used to derive properties of the components of the Cepheid systems. The colors of the companion candidates show a change in distribution at approximately 2000 au separations, from a range including both hot and cool colors for closer companions, to only low-mass companions for wider separations.

1. Introduction

Binary and multiple systems are very common products of star formation. This is increasingly so for more massive stars. Properties such as separation, mass ratio, and eccentricity are the "footprints" of star formation, providing observational insight into the process. Separations between components of the systems determine which observational approaches can be used to study them, as summarized by Figure 1 in Sana (2017). These include radial velocities for close binaries and many new techniques for resolving more distant companions. Duchêne & Kraus (2013) provide a recent summary of observations of multiple systems. Evolution of systems can occur at the pre-main sequence phase or post-main-sequence phase through Roche-lobe overflow and the dynamical interaction. Formation

and evolution of massive stars in multiple systems is particularly complex (de Mink et al. 2014), and a high fraction of O stars undergo interaction and mergers. The formation scenario in multiple systems probably involves core fragmentation, leading to relatively wide separations followed by disk fragmentation for closer components and subsequent migration for very close components. Complex multiple systems, however, can be produced by more than one scenario (Tokovinin 2018a).

The formation of wide binaries presents a puzzle. The most likely scenarios are the unfolding of triple systems (Reipurth & Mikkola 2012), the dissolution of clusters (Kroupa 1995), and the formation from adjacent cores (Tokovinin 2017).

As we are increasingly realizing, O and B stars often occur in systems with more than two stars, inevitably making the discussion of individual systems somewhat complicated. Cepheids (former B stars with typical masses of $5\,M_\odot$) fall in the lower part of the mass range of O and B stars. However, there are several features of Cepheid systems that mean that they make an important contribution to an accurate picture of

the distribution of masses and separations in multiple systems. They are a well-defined sample of evolved helium-burning stars. They are less rare than O stars, providing more examples that can be resolved by interferometric techniques. The combination of a cool evolved star and a hot companion leads to uncontaminated spectra of both the brightest and hottest stars in the system at different wavelengths. Finally, Cepheid parameters are easier to relate to their main-sequence B-star counterparts than more massive stars because mass loss on the main sequence is minimal. However, formation and the main-sequence stages for Cepheids are not the end of the story. From B-star binary statistics we know that approximately one-third of Cepheids are the products of mergers (Sana et al. 2012; Moe & Di Stefano 2017). This is a good example, however, of a complication that we have information to understand because it will only have affected short-period main-sequence binaries. In addition to understanding how multiple systems are formed (and what they tell us about the process), multiple systems, especially those containing massive stars, are important in many exotic end-stage objects. They are implicated in creating many objects such as X-ray binaries, millisecond pulsars, supernovae, Algols, and perhaps gamma-ray bursts and gravitational radiation sources. Moe & Di Stefano (2017) review binary properties involved in such outcomes.

The current study is part of a series aimed at determining the binary or multiple properties of Cepheids. The first paper (Paper I; Evans et al. 2013) is a discussion of the binary properties of a group of Cepheids with mass ratios greater than 0.4, compiled from a list observed by the International Ultraviolet Explorer (IUE) satellite. This list is equally sensitive to companions at any separation, making the distribution of separations unbiased. The second paper discusses a sample of 70 Cepheids observed with the Hubble Space Telescope (HST) Wide Field Camera 3 (WFC3) in two filters (Paper II; Evans et al. 2016a). This paper discusses candidate companions more distant than 5″, where photometry of possible companions is not contaminated by the much brighter Cepheid. The current paper (Paper III) follows with a discussion of possible companions closer to the Cepheid. These studies are supplemented with a discussion of XMM-Newton X-ray observations of systems with possible companions, in order to determine whether the companion is young and active enough to be a physical companion of the Cepheid (Paper IV; Evans et al. 2016b). The study of resolved companions is complemented by a discussion of radial velocities for northern Cepheids (Evans et al. 2015).

The sections below discuss the observations and data reduction for Cepheids with companions separated between 2″ and 5″ and also for companions within 2″. Chandra X-ray observations are then used to verify the companions. The discussion section summarizes candidate companions at all separations. Special attention is given to companions within 2″, and the components of these complex systems are discussed in detail. This includes the color–magnitude diagram (CMD), the distribution of colors as a function of separation, and inner binaries of this group. Astrometric data from Gaia are used to identify wider companions, both gravitationally bound companions and comoving but unbound companions.

2. Observations and Data Reduction

Observations were made in our HST WFC3 snapshot program, which imaged 70 of the brightest Cepheids. The F621M and F845M filters were used; these can be transformed into the V and I bandpasses of ground-based photometry. (Throughout this paper all magnitudes discussed are in the Johnson-Kron-Cousins system.) Observations were made in a dithered sequence. The survey is described in Paper II, including the target list. The aim was to identify possible companions of the Cepheids, which are typically many magnitudes fainter. Because the point-spread function (PSF), dominated by the bright Cepheid, is complex, our data analysis has been divided into three sections, according to the angular distance from the Cepheid. For the area ⩾5″ from the Cepheid, the background is modest and only changes slowly, and hence photometry is straightforward to derive using standard tasks in IRAF.[15] The results for this separation range are discussed in Paper II.

In the current paper, we only treat the region within 5″ of the central Cepheid. We subdivide this inner region again into two zones. Between 2″ and 5″, we again perform simple photometry with standard IRAF tasks (Section 3). The innermost regions are dominated by the bright Cepheid, where its extended PSF makes it challenging to perform source detection and measure photometry. In Section 4 we describe this in detail.

3. Companions between 2″ and 5″

Source detection and photometry between 2″ and 5″ separation from the Cepheid was made in the same way as for the more distant companions; details are provided in Paper II.

Once the list of sources between 2″ and 5″ had been generated, we tested them for the appropriate combination of magnitude and color for main-sequence stars at the distance of the Cepheid, as in Paper II. For the main-sequence relation, we used the Dartmouth Stellar Evolution Database[16] to generate an isochrone for a 1 Gyr age for the pair of WFC3 filters we used, i.e., F621M absolute magnitude versus F621M−F845M color. Although this age—the minimum contained in the Dartmouth database (at the time of Paper II)—is older than that of the Cepheids (typically 50 Myr), even the most deviant stars in this study (the late-K spectral-type stars) are only ∼0.1 mag above this representation of the zero-age main sequence (ZAMS). To compare this ZAMS with the observed WFC3 photometry, we have reddened the color and absorbed the magnitude and moved it to the distance of the Cepheid. Full details (including the distances of the Cepheids) are provided in Paper II.

To select candidate companions of the Cepheids, we required them to lie within 2σ of a band lying between the ZAMS and a parallel line 0.75 mag above it (to allow for binaries). These candidates are listed in Table 1. Appendix A contains figures that illustrate the WFC3 images for the candidates in Table 1, and plot the CMDs for each field. The present paper focuses on possible companions within 5″; consequently, there are some additional stars within the ZAMS band that lie at larger separations from the Cepheid; these were discussed in the previous paper (Paper II).

Photometry of the candidate companions is listed in Table 1. The instrumental magnitudes have similar errors to those of more distant companions in the previous study derived from

---

Table 1
Candidate Cepheid Companions at Separations Between 2″ and 5″

F621M (mag)	F621M −F845M (mag)	V (mag)	V − I (mag)	Sep. (arcsec)	P.A. (°)	Sep. (au)
		Y Car				
16.45 ± 0.02	0.60 ± 0.02	16.91	0.93	2.6	55	3820
16.79 ± 0.03	0.86 ± 0.03	17.40	1.29	3.2	112	4700
		V496 Aql				
18.39 ± 0.09	1.56 ± 0.09	19.05	1.99	4.3	78	4250
		TT Aql				
17.16 ± 0.05	1.40 ± 0.05	17.82	1.85	3.8	67	3520
		V350 Sgr				
17.24 ± 0.04	1.31 ± 0.04	17.91	1.77	3.1	128	2780
		BB Sgr				
17.41 ± 0.06	1.31 ± 0.07	18.08	1.77	3.3	158	2740
		RV Sco				
15.37 ± 0.01	0.90 ± 0.01	16.00	1.34	3.6	173	2710

the statistics. However, we expect that there is some additional uncertainty due to a more variable background. Table 1 lists the instrumental F621M magnitude (F621M) and color (F621M −F854M; Columns 1 and 2). For convenience, these magnitudes have been transformed to ground-based V and $V - I$ using the relations in Paper II (Vegamags), and they are given in Columns 3 and 4. The separation in arcsec, the position angle, and the projected separation in au (using the distances to the Cepheids from Paper II) are listed in Columns 5, 6, and 7. (For V496 Aql, the position angle has been corrected in Table 1 from than that in Table 5 in Paper II.)

4. Companions Within 2″

4.1. Data Reduction

For these close companions lying within the PSF wings of the bright Cepheid primaries, we proceeded as follows. The data processing started with the geometrically distorted, flat-fielded individual frames (FLT images) from the HST archive. We then applied a custom data-reduction procedure to deal with saturation and charge bleed.

4.1.1. Masking the Charge Bleed

The Cepheids are severely overexposed in our frames. Not only are the central pixels saturated, but the additional charge collected beyond saturation bleeds out to adjacent pixels. This happens predominantly along the columns of the CCD. In the vicinity of the Cepheid, pixels that are bled into also reach the saturation charge limit, and are flagged by the pipeline appropriately. However, we find that charge continues to bleed upward and downward along the columns, leading to severely enhanced charge levels up to two pixels beyond the fully saturated region. In addition, charge bleeds to the right (increasing x value in image coordinates) into the neighboring column. We thus add custom filtering to any pixel that is found to the right or one or two pixels above or below a pixel that is already marked as saturated by the standard pipeline. Gilliland et al. (2010) performed a similar analysis and suggested increasing the region masked due to saturation by one pixel in any direction. In our data, on the one hand, this recipe leads to spurious enhanced emission above and below the bleed region where charge bleeds more than one pixel beyond the fully

saturated region. On the other hand, it masks out area to the left of the saturated regions that seems usable.

4.1.2. Combining Exposures

We combined individual exposures for each filter and each object using `astrodrizzle` from DrizzlePac (Hack et al. 2013). This algorithm projects the values of all contributing exposures onto the sky, and then, for every sky position, averages over all valid (non-masked) values. Because the individual exposures have slightly different boresight coordinates, pixels fall onto the sky differently. Thus, this procedure results in a smaller area masked due to bleed than in the individual images. On the other hand, close to the Cepheid, only one of three exposures might contribute valid data, while all three images are averaged at larger distances. Because the signal close to the Cepheid is high, the noise in the combined image is still acceptable. We chose 0″0396 as the pixel size in the resampled images.

4.1.3. Cutting Out Subimages

In this section, we concentrate on close companions within 2″. Because the Cepheids are all well saturated, we cannot determine the position of peak flux. Instead, we fit straight lines to the diffraction spikes (diagonals in our images) and take the intersection of the diffraction spikes as the position of the Cepheid. We then extract subimages 120 pixels on each side, centered on the Cepheid. Based on the uncertainties of the fit to the diffraction spikes, we estimate that this procedure is accurate to about one pixel.

4.2. PSF Subtraction and Fitting

Sources more than 2″ from the Cepheid are discussed in Paper II and Section 3 above. In this section, we study the region within 2″, where the image is dominated by the PSF of the Cepheid.

4.2.1. Locally Optimized Combination of Images (LOCI)

In order to detect and perform photometry on potential companions, we need to subtract the PSF of the Cepheid itself. This is challenging because the HST PSF changes with time. Several observational and computational approaches to detect faint sources close to a much brighter primary have been developed in the past years, especially with an application to exoplanets. One of the most common observational techniques is angular differential imaging, where the same source is observed more than once with a different orientation of the instrument, such that instrumental features rotate on the sky, but true companions are fixed in sky coordinates. The scheduling of a snapshot program did not allow for this approach, so we are limited to computational methods to reduce the impact of the Cepheid PSF. Lafrenière et al. (2007) introduced a method called LOCI; see their paper for a mathematical description of the algorithm. In short, this algorithm describes an image as a linear combination of companion-free reference images. The coefficients that lead to the smallest residual between target image and the combination of reference images can be found essentially by a matrix inversion, which is computationally more efficient than numerical function minimizers. Fitting the whole image at once would introduce two major problems. First, the temporal
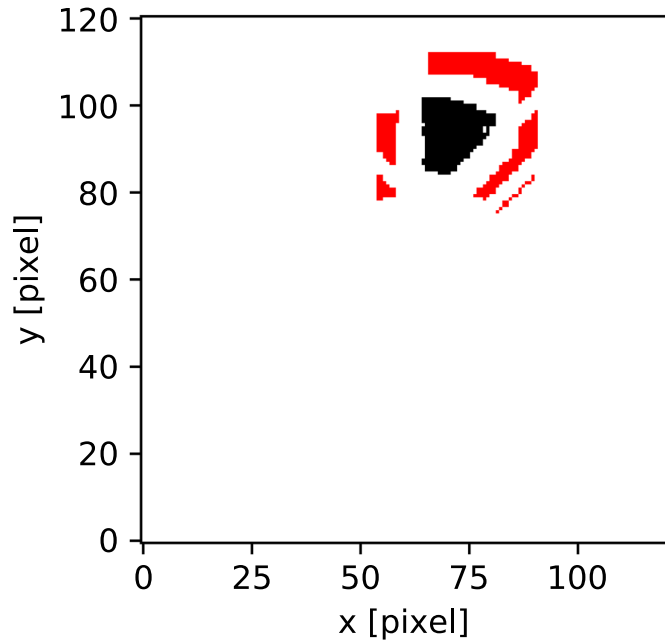
Figure 1. Example of an optimization region in LOCI. To find the best possible combination of the PSF templates for the black region, we actually fit in the red region. In this way, a moderately bright point source in the black region does not impact the results of the fit. Note that the red region does not completely envelop the black region, but has gaps avoiding regions that are contaminated by bleed or diffraction spikes or where one of the reference images cannot be used because it has a candidate companion itself.

change in the PSF might depend on the position, e.g., some parts of the PSF change more than others due to a temperature change of the telescope. Describing the full image at once thus requires a large number of reference images. Second, if a companion exists and is included in the fit, the fit will try to subtract it as much as possible, compromising the photometry. Thus, for LOCI the image is divided into several smaller regions. To find the best linear combination of templates for a specific region, we perform the optimization on an area that is outside the region of interest (see Figure 1).

4.2.2. Modification of Standard LOCI Procedures

Several enhancements of the LOCI method developed by Lafrenière et al. have been suggested in the literature, including template LOCI (Marois et al. 2014), which considers spectral information, or matched LOCI (Wahhaj et al. 2015), which inserts artificial point sources with known properties to inform the fitting process. Another approach is to decompose the set of PSF templates into eigenimages, thus using information from all images to isolate the true PSF components and separate them from observational noise that varies from image to image (Soummer et al. 2012). After reviewing these ideas in the literature, we modified the basic LOCI algorithm for the specific characteristics of our data set.

For any one Cepheid observation, we use the set of the other 69 observations taken in the same filter in our program as template images. This is justified because they are all taken within a few months of each other, use an identical instrumental setup (except for the exposure time), and all expose the central source well into saturation, bringing out faint PSF features visible beyond 2″, which are generally hidden in the noise for other archival data taken in the same filter. The drawback of this method is that some of the template images
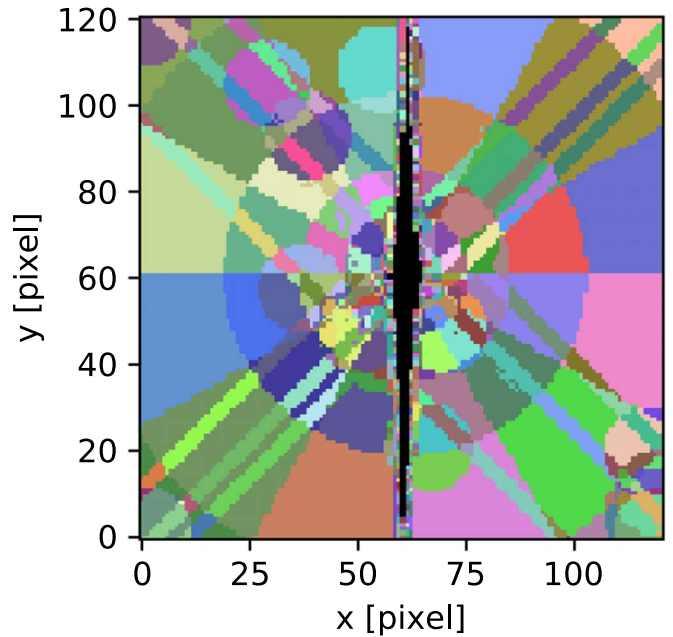

Figure 2. An image is typically divided into more than 500 regions for fitting. Each color shows one region. Apparent circle shapes (e.g., the circle centered on (55, 110)) are due to potential companions in one of the images, forcing a smaller set of templates in that region. Similarly, diagonal lines are due to diffraction spikes from bright companions that we masked.

might themselves contain companions, which would leave negative imprints on the reduced images. We thus perform an initial source detection (see next subsection) and mask regions potentially affected by a companion. For fits involving this region, only the remaining 68 images are used as templates. Similarly, the region affected by bleed differs from image to image. To perform a fit close to the central source, we used only those images that have valid data in this region as fitting templates. Following this prescription, a typical image in our data set is separated into more than 500 regions, each potentially with a different set of template images (Figure 2).

4.2.3. Initial Source Detection

The very brightest companions (see Table 2) are themselves saturated and are easily visible by eye. To identify other companions we need to mask before using images as LOCI templates, we construct a median image. The magnitude of the Cepheids is very different, and this is not fully compensated for by choosing different exposure times. The flux level in the images differs by about a factor of 1000 between the brightest and faintest image. We normalize each image by dividing the image by its median value. As a second step, we form a median image from all normalized images for each band. The median images show the shape of the average PSF, not including any companions. We then divide each normalized image by the median image. The result of this is an image that shows how each data set deviates from the median PSF. While not flux-conserving, this procedure works well to highlight potential companions. We use the `daofind` algorithm from Stetson (1987) as implemented in `photutils` to locate potential point sources and mask them before performing LOCI fitting. At this stage, we identify 17 potential companions and mask their positions in both filters. Not all of those sources will turn out to be real, but we can be conservative here because masking a potential source just means that only one image
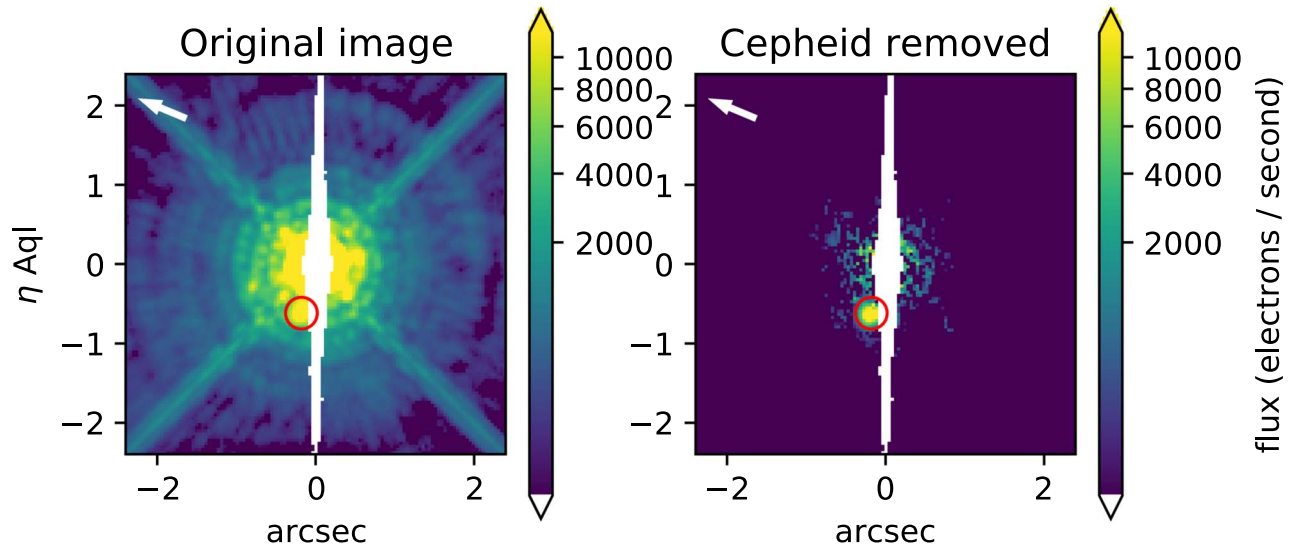
Figure 3. Image of η Aql in the F845M band. Several bright PSF features are seen within $1''$ of the Cepheid position. The image is oriented along the detector coordinates. The white arrow points north. Right: the companion is clearly visible after the LOCI subtraction.

Table 2
Candidate Companions Detected after PSF Correction

Cepheid	Sep. (arcsec)	P.A. (°)	m_{621} (raw) (mag)	m_{621} (corr) (mag)	σ_{621} (mag)	m_{845} (raw) (mag)	m_{845} (corr) (mag)	σ_{845} (mag)
R Cru	1.9	344.5	15.43	15.36	0.03	14.41	14.33	0.02
U Aql	1.6	225.1	12.01	11.91	0.06	11.12	11.04	0.04
U Vul	1.5	319.7	16.26	16.18	0.04	14.92	14.85	0.03
S Nor	0.9	259.2	11.69	11.40	0.49	11.47	11.20	0.43
V659 Cen	0.6	234.9	10.54	⋯	⋯	10.12	⋯	⋯
η Aql	0.7	95.7	9.34	⋯	⋯	8.90	⋯	⋯
AX Cir	0.3	332.4	7.24	⋯	⋯	6.98	⋯	⋯
AV Cir	2.1	288.5	20.11	20.00	0.03	19.19	19.10	0.07
BG Cru	3.1	294.8	15.52	15.11	0.08	14.90	14.70	0.04
CO Aur	2.8	8.8	18.65	⋯	⋯	17.66	⋯	⋯

cannot be used as PSF template in one region (see Figure 2 for an example), which has little impact on the quality of the fit given that the set of potential templates consists of 69 images.

4.2.4. Application of LOCI and PSF Fitting

We perform LOCI fitting to each of our images and subtract the result of the best fit in each region from the original image. Figure 3 shows an example. Most of the PSF features, including the diffraction spikes, are significantly reduced, but within about $1''$ from the Cepheid, residuals from the subtraction increase. We find that source-detection algorithms do not perform well in this region. We thus inspect every image by eye and perform PSF photometry on all source candidates from Section 4.2.3. In principle, our procedure requires iteration, where any new sources identified would now be masked and the LOCI fitting repeated. However, no new sources beyond the previous candidates are identified. Table 2 lists the resulting source detections.

4.2.5. Uncertainty Estimates

The uncertainty of the properties of the companion is dominated by systematics introduced through the LOCI

subtraction. Additionally, there is a risk of oversubtraction in the LOCI procedure. We quantify those effects through simulations in which we insert fake sources with known fluxes into the images, run the same LOCI subtraction, and measure the flux of the detected companions. From our images, we select sources that are not visibly impacted by the PSF of the Cepheid. We checked the Gaia Data Release 2 (DR2) catalog (Gaia Collaboration et al. 2016, 2018) for these sources. While this release does not explicitly mark extended or multiple sources, the errors on the coordinates are a good proxy. We reject any sources with Gaia coordinate errors above 0.1 milliarcsec as likely binaries. We fit a beta function as analytical PSF to the remaining sources and reject sources when the fit parameters are significantly different than the sample mean. We finally have a set of 18 PSF template stars. We fix the parameters of the shape and use the resulting analytical PSF for fits to both the real data (Section 4.2.4) and the LOCI-subtracted images with simulated companions inserted.

For each template star, we extract squares 25 pixels wide centered on these sources from background-subtracted images. For each simulation, we select one of these sources, scale its F621M and F845M flux as required, and add it to one of the original Cepheid images. We then perform LOCI subtraction
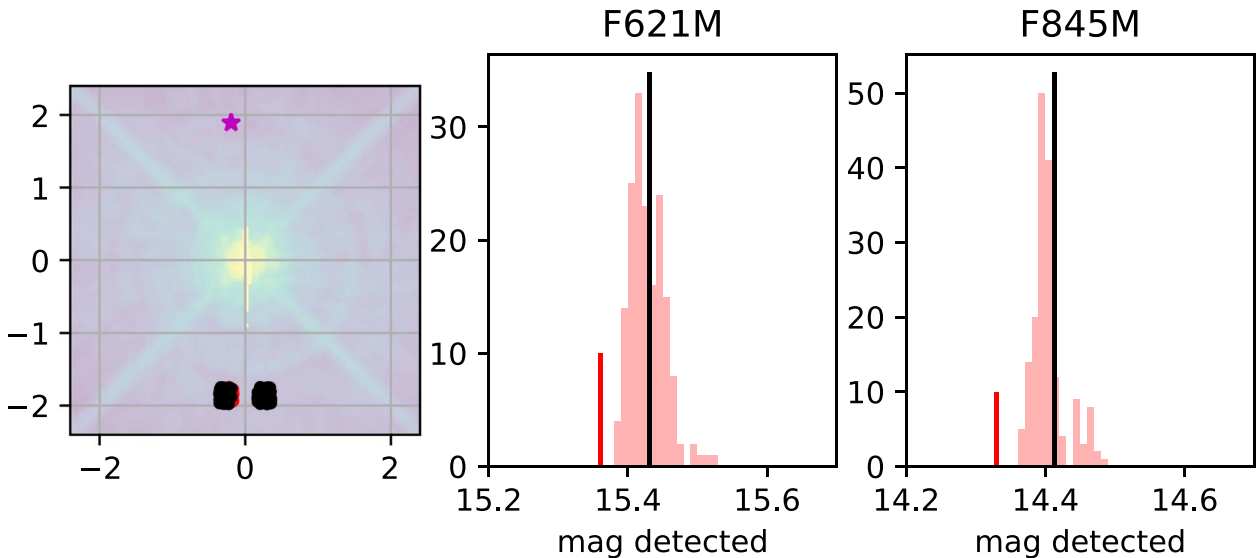
Figure 4. Left: image of R Cru in the F621M band. The image is oriented along the detector coordinates. The purple star marks the location of the detected companion. Simulated companions are inserted at a location where the PSF of the Cepheid is comparable, here below the Cepheid at a similar distance to Cepheid and bleed column. Black dots are inserted companions that are recovered by the fit procedure, red dots are companions that are not recovered (e.g., because they are located too close to the bleed column). Center and right: histogram of the recovered magnitudes of inserted companions for each filter. The red line marks the true magnitude of the inserted companions, and the black line shows the measured magnitude of the companion in the real image.

on the image with the artificially inserted companion and measure the source flux through PSF photometry. For each source in Table 2 we run 200 simulations. Depending on the position of the companion in Table 2, we select positions that are similarly effected by the Cepheid PSF. For instance, for R Cru, where the companion is found almost $2''$ from the Cepheid but only a few pixels from the bleed column, we inject the artificial companions into the image at the opposite side of the Cepheid with a similar distance to the bleed column (Figure 4) and vary the insert location slightly to probe any background fluctuations statistically. Typically, some of the companion flux is subtracted in the LOCI procedure, and thus the measured magnitudes (pink histograms in Figure 4) are fainter than the input magnitudes (red line). We thus conclude that the true flux of the companion in the real image must also be higher than the measured flux, and we apply the offset determined from the simulations to correct the measured companion magnitude (black line). We take the standard deviation of the simulated magnitudes as the error estimate for the companion flux because the distribution of magnitudes is typically peaked, but the distribution has a significant tail toward fainter magnitudes for S Nor, which means that the true magnitudes could be up to 0.5 mag brighter than the number given in Table 2.

4.2.6. Saturated Companions

This procedure cannot be applied for the very brightest companions that are themselves saturated because we do not have PSF template stars of comparable brightness. If the companion's core is saturated, PSF photometry can in principle determine the flux by fitting the wings of the PSF. However, our template stars are not bright enough to determine the shape of the wings accurately enough. Similarly, the template stars would have to be scaled up significantly to be inserted into images for our simulations that determine the flux uncertainties, but this would significantly enhance the noise. However, for a measurement of the position alone, the exact shape of the PSF
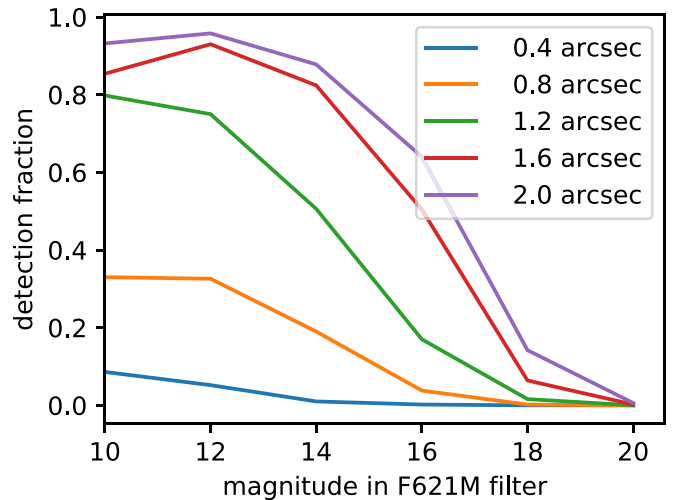

Figure 5. Detection fraction for companions depending on distance from the Cepheid and flux from the companion.

wings is not important, and we thus provide positions for the saturated companions in Table 2.

4.3. Results

4.3.1. Completeness

To quantify our detection limits, we employ a procedure similar to our uncertainty estimate for detected companions. We insert companions into Cepheid images at a certain radius from the Cepheid, apply our source-detection algorithm, and measure the fraction of companions recovered in both bands. The inserted companions have a color $m_{621} - m_{845} = 1$, similar to the values observed in the detected companions (Table 2). We verified that the detection fraction changes little for reasonable choices of this color. Figure 5 shows the limits. We note that these limits describe the detectability in our whole sample. The flux level at a given distance from the Cepheid

Table 3
Properties of Candidate Companions Detected after PSF Correction

Cepheid	Sep. (au)	V (mag)	$V - I$ (mag)	$(V - I)_0$ (mag)	$E(B - V)$ (mag)	Dist. (pc)
R Cru	1580	16.02	1.49	1.27	0.19	829
U Aql	981	12.53	1.30	0.90	0.35	613
U Vul	822	16.85	1.79	1.04	0.65	548
S Nor	819	11.55	0.30	0.08	0.19	910
V659 Cen	452	…		…	0.21	753
η Aql	191	…		…	0.12	273
AX Cir	158	…		…	0.25	527
AV Cir	1472	20.63	1.34	0.88	0.40	701
BG Cru	1615	15.42	0.64	0.58	0.05	521
CO Aur	2229	19.30 uc	(1.45)	(1.19)	0.23	796

differs by three orders of magnitude between the brightest and faintest image due to different exposure times and Cepheid magnitudes. A companion that could be detected in one image can therefore be hidden in the background in another. We note further (in the image segments we discuss outside of $0{.}''5$) that between $1''$ and $0{.}''5$, the bleed column obliterates a significant part of the image.

At $0{.}''4$, only a small fraction of companions is detected, even for the brightest sources. For bright sources, this number rises quickly with increasing distance, and beyond $1''$, most companions with $m < 12$ that do not overlap the diffraction spikes or the bleed columns are detected. Fainter companions require larger distances. Only for distances beyond $1''$ are more than half of the $m_{621} = 16$ companions detected.

4.3.2. Detected Companions

The images in which companion candidates were detected are shown in Figure 3 and in the figures in Appendix B before and after PSF correction.

Table 2 lists the detected companions. It gives both the raw, measured magnitude and the corrected magnitude based on the simulations. The uncertainty given is also taken from the simulations. No correction can be derived for the brightest three companions (around η Aql, V659 Cen, and AX Cir) because these companions are themselves saturated. Fluxes are highly uncertain, but separation and position angle only rely on the assumption that the PSF is rotationally symmetric. The uncertainties in the position angle, like the uncertainties in the fluxes, are dominated by residuals from the LOCI procedure. We analyze simulated inserted sources and find that essentially all inserted sources are recovered within 5 pixels ($0{.}''2$) of the inserted position, while the large majority of sources are found within half that distance. These are upper limits to the positional uncertainty for true companions because our insertion procedure can add sources only at integer-valued positions, introducing an additional shift up to half a pixel.

The photometry in Table 2 has been converted into V and I in the same way as in Paper II, using the corrected photometry. The results are listed in Table 3. Distance and reddening are also from Paper II, with the distance based on the Benedict et al. (2007) Leavitt Law. The separation in astronomical unit is also listed, based on this distance.

The LOCI search also identified three additional sources in the postage stamps, which are listed in the last three rows of Tables 2 and 3. In the case of BG Cru, the source lies on a

diffraction spike, and required LOCI processing to identify it. V and $V - I$ for CO Aur are based on uncorrected magnitudes in Table 3. However, when we use the distance to the Cepheid, all three companions are too faint to be consistent with a ZAMS relation. For BG Cru, for instance, the $(V - I)_0$ corresponds to an F8 V star (Drilling & Landolt 2000), which would have $M_V = + 4.0$. The V, $E(B - V)$, and distance, however, correspond to $M_V = +6.7$. We conclude that they are all chance alignments, and do not discuss them further.

4.4. Caveats

As discussed in Paper II, the goal of the survey was to detect companions down to dwarf K spectral types, which limits contamination by field stars.

As discussed below (Table 5), in a number cases an absolute magnitude from other sources, such as IUE spectra, is more accurate than the HST photometry for very close companions.

5. Chandra Observations

Analysis of the properties of members of the multiple systems containing a Cepheid frequently requires multiwavelength observations. X-ray observations are often an important diagnostic. Specifically, Chandra observations of two stars, R Cru and S Mus, follow up XMM observations in Paper IV with higher spatial resolution, providing additional information about the system components. The details of the observations are provided in Appendix C.

6. Discussion

6.1. Summary of Candidate Companions

Because of differences in the data-analysis procedures dictated by the angular separations, in the preceding work we divided the resolved companions found in our HST WFC3 imaging survey into three groups (separations $>5''$, $2''$–$5''$, and $<2''$). In the following discussion, we combine the first two groups, designating them the "resolved wide" companions. The latter group is called the "resolved close" companions. In terms of physical projected separations, the resolved wide companions lie more than $\sim$2000 au from the Cepheid, and the resolved close ones are closer to the primary star. We now examine whether the properties of the stars in the two groups differ.

Table 4 presents the results for the combined sample of 16 candidate companions. These data are assembled from Table 2 in Paper II for the top group, with separations greater than $5''$. For the middle group, with separations of $2''$–$5''$, the entries are from Table 1. The data for the close companions below $2''$ are more complicated, and these companions are discussed individually below. Our measures of separation and magnitude are listed in Tables 2 and 3. However, for very close companions and systems with multiple companions, the most reliable companion parameters come from several sources, which are discussed and assembled in Table 5. Table 4 lists the projected separations in both arcseconds and astronomical units, the V and $V - I$ magnitudes and colors, the dereddened $(V - I)_0$ color, the $E(B - V)$ reddening, and the distance. The distances and reddenings are from Paper II. As in Paper II, the $V - I$ color excess is found from the relation $E(V - I) = 1.15\,E(B - V)$.

Table 4
Summary of Resolved Candidate Companions

Cepheid	Sep. (arcsec)	Sep. (au)	V (mag)	$V - I$ (mag)	$(V - I)_0$ (mag)	$E(B - V)$ (mag)	Dist. (pc)
Resolved Wide							
			Separation $>5''$				
R Cru	7.6	6330	16.28	1.17	0.95	0.19	829
FF Aql	6.9	2520	11.22	0.85	0.60	0.22	365
AP Sgr	6.3	5320	17.85	1.72	1.50	0.19	845
RV Sco	6.0	4520	12.68	0.63	0.24	0.34	753
			$2'' <$ Separation $< 5''$				
RV Sco	3.6	2710	16.00	1.34	0.95	0.34	753
BB Sgr	3.3	2740	18.08	1.77	1.45	0.28	831
Y Car	3.2	4700	17.40	1.29	1.20	0.08	1468
Y Car	2.6	3820	16.91	0.93	0.84	0.08	1468
V350 Sgr	3.1	2780	17.91	1.77	1.40	0.32	896
Resolved Close							
			Separation $<2''$				
R Cru	1.9	1580	16.02	1.49	1.27	0.19	829
U Aql	1.6	981	12.53	1.30	0.90	0.35	613
U Vul	1.5	822	16.85	1.79	1.04	0.65	548
S Nor	0.9	819	11.55	0.30	0.08	0.19	910
η Aql	0.7	191	…	…	…	0.12	273
V659 Cen	0.6	452	…	…	…	0.21	753
AX Cir	0.3	158	…	…	…	0.25	527

Among the possible companions separated by more than $5''$ from the primaries, only five systems remained after we eliminated those candidates undetected in X-rays, implying that they are not young enough to be Cepheid companions. The remaining five are R Cru, FF Aql, AP Sgr, RV Sco, and TT Aql. The discussion in Paper II concluded that a Cepheid with a crowded line of sight (a field with more than two possible companions) is more likely to have chance alignments. On this basis, we remove TT Aql. The candidate companion of AP Sgr has the second-largest physical separation in the remaining sample, and it is a K dwarf, which is the most common type of field-star chance alignment. Thus AP Sgr is the most suspect of the remaining retained candidates in the list. As discussed in Appendix C, we retain the candidate wide companion for R Cru.

We also checked the Gaia DR2 catalog for parallaxes and proper motions of our candidate companions. Because the candidates are so close to the much brighter Cepheids, parallaxes are not available in most cases, particularly for the closer companions. The candidate companions of V737 Cen, R Mus, and Y Sgr were found to be much more distant than the Cepheids, consistent with the negative results of the X-ray observations reported in Paper IV; they are not included in Table 4. For the possible companions with separations $>5''$ in Table 4, the DR2 results are as follows. The Gaia DR2 parallax for R Cru itself is negative, but the parallax of the wider of its two candidate companions is consistent with the distance given in Table 4 (and with the Hipparcos parallax of R Cru), and its DR2 proper motion is similar to that of the Cepheid. The parallax of the FF Aql companion agrees within the errors with that of the Cepheid, but as noted by Kervella et al. (2019b), its proper motion is significantly different; this implies a relative velocity too high for it to be bound, unless it is itself a binary. The companion for AP Sgr is listed in DR2, but no parallax is given. Finally, the DR2 parallax for the wider of the two RV Sco companions agrees with that of the Cepheid within the errors, and its proper motion is similar.

The middle group in Table 4 lists the candidate companions with separations between $2''$ and $5''$. The only companion listed in Gaia DR2 is that of RV Sco, but no parallax or proper motion is given. In the case of V496 Aql, the DR2 parallax is significantly smaller (4.3σ) than that of the Cepheid, and hence is likely to be a chance alignment. It has been omitted from Table 4.

6.2. Resolved Close Companions: Companions Closer than $2''$

A number of the systems with a companion closer than $2''$ to the Cepheid have at least one additional component. This means that disentangling the mass and temperature of the companions often requires information from a number of techniques. Here we discuss what is known about the components of these close systems in the third group in Table 4. This becomes important below in first examining the CMD of the companions and subsequently the distribution of colors as a function of separation, and the multiplicity properties of the sample.

Because massive star systems often have multiple components, in Appendix D we provide considerable detail for each system. The parameters of each component (mass, temperature, and luminosity) can be derived using observations over a wide wavelength range, and also as a function of separation. Many approaches and tools are currently available to do this. Radial-velocity studies extend over many decades. The emphasis in this study is on separations on the $1''$ scale, but a number of systems have been observed via interferometry (e.g., Gallenne et al. 2019), accessing closer separations. Both HST and IUE provide information about hot companions in the satellite ultraviolet. Chandra and XMM X-ray observations test the ages of companion candidates. Finally, Gaia and Hipparcos data have contributed in two ways (Kervella et al. 2019a, 2019b). First, the comparison of proper motion from the two satellites in some cases results in proper-motion anomalies, indicative of orbital motion. Second, comoving companions can be

Table 5
Preferred Properties of Resolved Close Companions

Primary (Cepheid)	V_0 (mag) Comp	M_V (mag) Comp	Spectral Type Comp	$(V-I)_0$ (mag) Comp	Source	Reference[a]
R Cru	15.4	+5.8		1.27		(1)
U Aql	11.3	+2.4	A5	0.16[b]	HST/STIS	(2)
U Vul	14.6	+5.9		1.04		(1)
S Nor	10.89	+1.1	B9.5 V	−0.04[b]	IUE	(3)
V659 Cen	8.72	(−0.3)	B6.0 V	−0.16[b]	IUE	(3)
η Aql	10.0	+3.2	F3	0.44[b]	VLT/NACO	(4)
AX Cir	6.91	(−0.3)	B6.0 V	−0.16[b]	IUE	(5)

Notes.
[a] References: (1) Table 4, (2) Appendix D, (3) Evans (1992b), (4) Gallenne et al. (2014b), (5) Evans (1994).
[b] From Drilling & Landolt (2000), their Table 15.11 (which is quoted from Bessell 1979).

Table 6
Multiple Components in Systems with Resolved Close Companions

Cepheid	Multiple ID	Sep. (arcsec)	Sep. (au)	SB[a]	V_0 (mag)	M_V (mag)	Spec. Type	Reference[b]	Wide[c]
R Cru	AB	1.9	1580		15.4	+5.8	K	(1)	WB
	Aa,Ab		3:	SB			<A2	(9)	
	AC	7.6	6300		15.6	+6.0	K2 V	(11)	
U Aql	AB	1.6	981		11.3	+2.4	A5 V	(6)	
	Aa,Ab	0.107	66			+1.8	A3-4 V	(6)	
	Aa1,Aa2	0.0101	6.2	SB		+1.2	B9.8 V	(6)	
U Vul	AB	1.5	822		14.6	+5.8	K0	(1), (9)	
	Aa,Ab		7.1	SB			<A1	(3), (9)	
S Nor	AB	0.9	819		10.9	+1.1	B9.5 V	(1), (10)	WC
	Aa,Ab		8.87	SB:			F0 V	(3)	
	AC	14.6	13300		13.29	+3.5	G3 V	(11)	
V659 Cen	AB	0.6	452		8.7	−0.3	B6.0	(1), (9)	WB
	Aa,Ab		3:	SB				(5)	
η Aql	AB	0.7	191		10.0	+3.2	~F3 V	(1), (2)	
	Aa,Ab		1.3:	SB	8.39	+1.2	B9.8 V	(4), (8)	
AX Cir	AB	0.3	158		6.9	−0.3	B6.0	(1), (9)	WB, WC
	Aa,Ab	0.029	15.4	SB		+0.2	B9.0	(7), (12)	
	Ab1,Ab2							(7), (12)	

Notes.
[a] Spectroscopic-binary companion.
[b] References: (1) Table 5, (2) Gallenne et al. (2014a) (3) Kervella et al. (2019a) (4) Appendix C, (5) R. I. Anderson (2020, in preparation), (6) Appendix D, (7) Gallenne et al. 2014b (8) Evans (1991), (9) Evans (1992a), (10) Evans (1992b), (11) Paper IV, (12) A. Gallenne et al. (2020, in preparation).
[c] Wide companion types: WB gravitationally bound; WC comoving.

identified and classified either as bound or unbound. These data are discussed further in Section 6.9, "Gaia Components."

In the discussion of some of the systems we have estimated masses of the companions. The approach used is discussed in Evans et al. (2018), based on data from detached eclipsing binary systems (Torres et al. 2010). In particular, because the companion to a more massive primary should not have evolved significantly, the lower envelope to the temperature–mass data is used.

Magnitude measurements for sources within $2''$ of the Cepheid have substantial uncertainties. This is particularly important in determining the color or temperature using the difference of two filters, resulting in an uncertainty that is a significant fraction of the range of color. In many cases for the companions, there is an alternate measurement that provides a more accurate color or temperature. Specifically, many of the stars have an IUE spectrum, which provides a sensitive determination of the spectral type of the companion; the

companion can completely dominate the flux at 1500 Å. Table 5 summarizes the best ("preferred") combination of V_0 and $(V-I)_0$ available for the companions within $2''$ of the Cepheid. V_0 is taken from Table 3 for S Nor, R Cru, U Aql, and U Vul. From this, and the distance in Paper II, M_V is computed (Column 3). Column 4 is the spectral type from the instruments and literature references in Columns 6 and 7. Additional details are given for each star in Appendix D. The closest companions, V659 Cen B and AX Cir B, provide magnitudes that are too uncertain in the WFC3 images, so the value of M_V based on the IUE spectral type has been substituted. For η Aql, the M_V from the VLT/NACO imaging is provided in Appendix D.

This information for complex systems is discussed in Appendix D. We summarize the component parameters in Table 6 for reference. This includes the resolved companions (Table 5), as well as inner spectroscopic binaries and possible wider system members. While there is much detail in the linked inferences, the available observations provide well-constrained
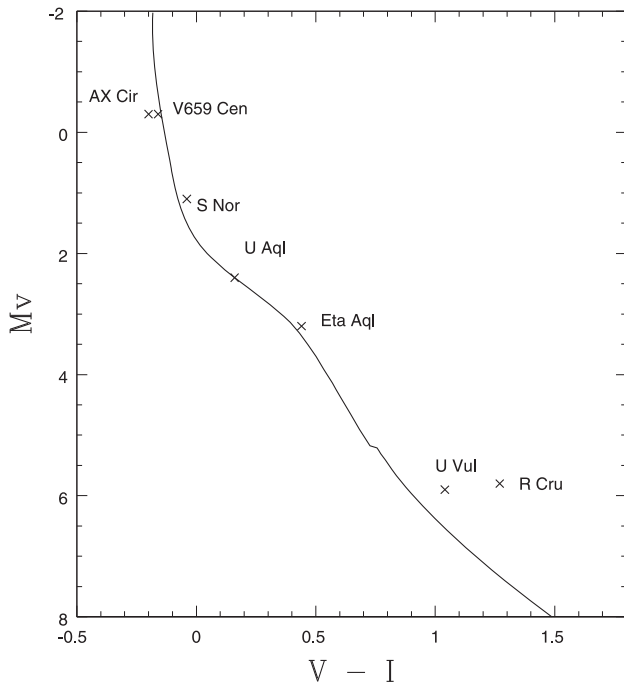
Figure 6. The M_V vs. $(V - I)_0$ color–magnitude diagram for the resolved close companions (Table 5). Colors and magnitudes are from Table 5, for which most are taken from WFC3 images. For η Aql, the data are from Gallenne et al. (2014a), although they agree with the WFC3 data. For AX Cir and V659 Cen, data are from IUE spectra. Identifications of the stars are included in the plot. The solid line is the ZAMS from Paper II.

properties for most of the stars involved. The top entry for each Cepheid is for the resolved companion identified in this study. The second column is the binary or multiple star notation. V_0, $(V - I)_0$, and M_V are taken from Table 5. The final right column lists results for very wide companion candidates from Gaia DR2 (Kervella et al. 2019b), where WB signifies bound companions, and WC are comoving companions. Systems in Tables 5 and 6 are ordered by decreasing separation of the resolved companion.

The important characteristic that emerges from the discussion of the complex systems is that all the systems with resolved close companions (companions within 2″) have an interior spectroscopic binary (or at least one is strongly suspected, in the case of S Nor). This is discussed in more detail in Section 6.6.

6.3. Resolved Close Companion Properties: CMD

We now return to a discussion of the close but resolved companions (Table 5), which are the first entry for each of the systems in Table 6, as discussed in Appendix D. As a first step in assessing the properties of the resolved close companions (within 2″ of the Cepheid (Table 5)), we consider the CMD (Figure 6), which provides a first examination of the properties of these companions. The companions are fairly evenly distributed in color, M_V, and hence in mass. Unlike the field initial mass function (IMF), they are not concentrated at low-mass stars. For wider companions, comparisons with the ZAMS are the way physical companion candidates are identified. In Figure 6 this is only a test for the two coolest companions, R Cru and U Vul because they are the only ones that are based on WFC3 photometry. While these points sit

above the ZAMS, indicating some errors, they are consistent with the companions being low-mass stars.

6.4. Systems with a Resolved Wide Companion (Wider than 2″)

Because the systems with a companion closer than 2″ have the distinctive property of an inner spectroscopic binary (Table 6), we examine the multiplicity properties of the systems with a companion wider than 2″ to see if they share this characteristic. Components of these systems are summarized in Table 7. Unless discussed below, the spectral types for the companions are derived from $(V - I)_0$ in Table 7, using the calibration of Drilling & Landolt (2000), their Table 15.11. The details of the components of these systems are discussed in Appendix F.

The possible companions with separations larger than 2″ are more likely to contain a line-of-sight coincidence with an unrelated field star than the inner group. However, of the six Cepheids for which a possible companion has been identified in this group, five have strong evidence of an inner spectroscopic binary, and only for one (BB Sgr) is an inner binary questionable and it is a cluster member. That is, the resolved wide systems share this characteristic of the resolved close companions. This is an additional property consistent with physical system membership.

6.5. Distribution of Colors

Ultimately, we wish to examine the properties of possible companions as a function of the (projected) separation in astronomical units, which is shown in Figure 7. Companion candidate properties are taken from Table 5 when available, or from Table 4.

Companion candidates closer than 2000 au span the full range of $(V - I)_0$. The hottest companion candidates, however, do not occur at larger separations. The hottest of the more distant companions, FF Aql and RV Sco (with $(V - I)_0$ colors corresponding approximately to G0 and A7 dwarfs, respectively) have evidence that they are associated with the Cepheid (Appendix F). The other companion candidates with separations larger than 2000 au are all cooler (approximately K0 or later). Thus there appears to be a trend in the color or temperature and mass of the companion candidates to lower mass stars at wider separations. This raises the question whether wider companions actually are preferentially less massive (or have been dynamically widened), or whether they are chance alignments with field stars or possibly a mixture of both.

One of the goals of this study is to determine how far from the Cepheid physical companions occur. The diminishing number with separations greater then 6000 au is consistent with the results of X-ray studies to identify active stars young enough to be Cepheid companions. X-ray observations of 14 of the 39 Cepheids with companion candidates with separations greater than 2″ in Paper II were discussed in Paper IV. The only two Cepheids with X-ray confirmed companions greater than 6000 au were R Cru (above) and S Nor. However, because S Nor is in a cluster, the X-ray source may be a cluster member rather than a gravitationally bound companion. Possible wide but bound companions revealed by Gaia are discussed in Section 6.9. Seven Cepheids in the WFC3 survey (δ Cep, AX Cir, AW Per, V350 Sgr, V659 Cen, BP Cir, and V950 Sco) have possible companions (Tables 9 and 10), as does the

Table 7
Multiple Components in Systems with Resolved Wide Companions

Cepheid	Multiple ID	Sep. (arcsec)	Sep. (au)	SB[a]	V_0 (mag)	$(V − I)_0$ (mag)	M_V (mag)	Spec. Type	Reference[b]	Wide[c]
AP Sgr	Aa,Ab		12:	SB:				⩽A5	(5), (2), (4)	
	AB	6.3	5320		17.19	1.50	+7.56	K7	(3)	
Y Car	Aa,Ab	0.0025	3.6	SB				B9.0 V	(6), (7), (4)	WC
	AB	2.6	3820		16.63	0.84	+5.80	K0	(3)	
or	AB	3.2	4700		17.12	1.20	+6.29	K5	(3)	
RV Sco	Aa,Ab		14:	SB				<A3	(4), (2)	
	AB	6.0	4520		11.50	0.24	+2.12	A7 V	(3)	
or	AB	3.6	2710		14.82	0.95	+5.44	K2 V	(3)	
V350 Sgr	Aa,Ab	0.0030	2.7	SB				B9.0 V	(8), (9)	WB, WB
	AB	3.1	2780		16.80	1.40	+7.04	K6	(3)	
BB Sgr	AB	3.3	2740		17.11	1.50	+7.51	K7	(3), (4), (5)	
FF Aql	Aa,Ab	0.0082	4.5	SB				K0	(1), (4)	
	AB	6.9	2520		10.46	0.60	+2.65	G0 V	(3)	

Notes.
[a] Spectroscopic-binary companion.
[b] References: (1) Gallenne et al. (2019), (2) Evans (1992a), (3) Table 4, (4) Kervella et al. (2019a), (5) Szabados (1989), (6) Petterson et al. (2004), (7) Evans et al. (2005), (8) Evans et al. (2018), (9) Kervella et al. (2019b).
[c] Wide companion types: WB gravitationally bound; WC comoving.
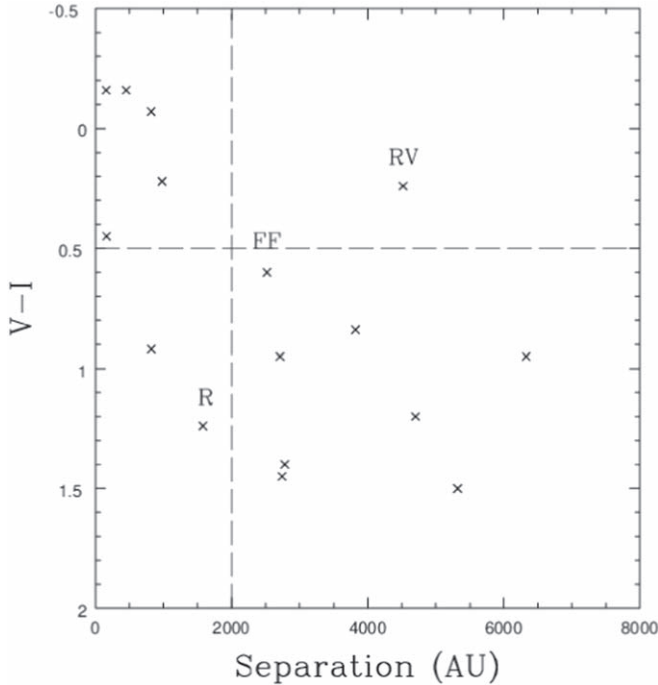
Figure 7. Colors and separations of the resolved close companions from the Cepheids. $(V − I)_0$ is in mag. The horizontal and vertical dashed lines are arbitrary divisions of the companion properties for discussion purposes. A component of the R Cru, RV Sco, and FF Aql systems is indicated.

Figure 8. Schematic of the separations of companions from the Cepheids for resolved close companions (within 2″) from Table 6. The vertical dashed line separates the spectroscopic companions (to the left of the line) from the resolved companions (to the right). Blue (large) and red (small) symbols represent companions earlier and later than A0, respectively. S Nor (below the horizontal dashed line) is a cluster member and more difficult to interpret.

cluster Cepheid U Sgr. This indicates further extended low-density companions.

6.6. Multiplicity

The group of stars with resolved close companions contains companions that are highly likely to be physically related to the Cepheid. As discussed above, the systems are complex, and it requires a number of approaches in addition to the HST WFC3 observations to assemble a picture of the masses and separations of the components. Table 6 summarizes the

information on the members of each system. In addition, as discussed in Section 6.9, Kervella et al. (2019b) used Gaia data to identify wide companions from distances and proper motions and test whether they are likely to be gravitationally bound to the Cepheid. The final right-hand column in Table 6 indicates

whether a wide bound (WB) or wide comoving (WC) companion candidate was found.

Figure 8 further summarizes the components schematically. We stress that it was developed from the list of Cepheids with resolved companions at separations of typically a few hundred astronomical units (Table 6). It is striking that in the Cepheid list compiled in this way, all have evidence of an inner binary, often with a known orbit. As noted above, because S Nor is in a cluster, it may have a different history of formation or interaction than the field stars and also possible chance alignments with cluster stars. Precise masses are not available for all the companions; however, limits or estimates can often be made from spectral types (Table 6). Figure 8 shows the masses schematically either as comparable to the Cepheid itself (a B star: large blue squares) or a lower mass A, F or G star (small red squares). While this is a crude division, several things are apparent in Figure 8. There is a variety in the component masses. For instance, R Cru and U Vul have only lower mass companions, whereas other systems have a mixture of masses. For AX Cir and V659 Cen, the most massive companion is not the closest companion (Section 6.2). The more massive companions are typically the closer ones, although AX Cir and V659 Cen are exceptions. This might be due to the formation process or subsequent dynamical evolution.

It is surprising that all the systems with resolved close companions in Table 6 also have an inner binary system, or at least a suspected one. This is markedly different from the fraction of spectroscopic binaries among Cepheids with periods shorter than 20 yr, which is $29\% \pm 8\%$ (Evans et al. 2015), less than one-third of a Cepheid sample. In a scenario in which systems with wider separations are formed before more closely separated components (in a process such as core fragmentation and subsequent disk fragmentation) it is hard to explain how wide components "know" that an inner binary will be formed later. A more probable explanation for the requirement that a wide component in Figure 8 has an inner binary is that the wide component of the triple (or higher) system was moved outward through dynamical interactions.

The resolved close companions in Figure 8 all appear to be distant third stars in triple systems. Because they are the closest resolved companions in the survey, they are the most likely to be gravitationally bound to the Cepheids. However, the striking result in Figure 8 of inner spectroscopic binaries encouraged us to check the slightly more distant resolved wide companions (from 2″ to 7″). System parameters are summarized in Table 7 and represented schematically in Figure 9. The system summaries in Figure 9 have been simplified in two ways. For two stars from Table 7 (RV Sco and Y Car), there are two possible companions in this range. Because it is dynamically unlikely that they are both system members because they are at very similar apparent separations, Figure 9 shows only the one considered to be the most probable. Second, wider companions discussed below are not shown. From the discussion of the Cepheids with resolved wide companions above (Table 7), all except for BB Sgr have good evidence of an inner spectro-scopic-binary system. In addition, as with S Nor, BB Sgr is a cluster member. This provides an alternative possibility for the resolved wide companion, a chance alignment with a cluster member, rather than a bound system member. It is also notable that the outer companion is significantly less massive than the Cepheid. This again fits the picture that a resolved companion
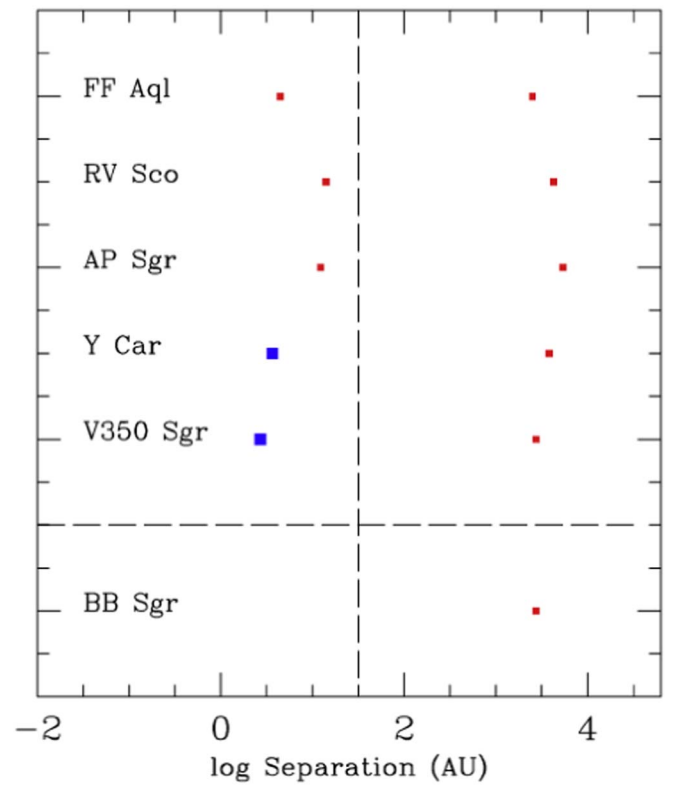

Figure 9. Schematic of the separations of companions for resolved wide companions (wider than 2″). Symbols are the same as for Figure 8. BB Sgr (below the horizontal dashed line) is a cluster member.

with a projected separation of several thousand astronomical units was moved outward through dynamical interactions within the triple system.

6.7. Dynamical Stability

The inner spectroscopic binaries for the 13 Cepheids in Tables 6 and 7 certainly have long-term dynamical stability with respect to the resolved companions from the WFC3 survey because of the very different orbital periods. However, two stars in Table 7 (RV Sco and Y Car) have two companions that have separations from the Cepheid that correspond to period ratios much lower than 5, found by Tokovinin (2018b) in stable triple systems. Anticipating the Gaia results for likely wide but bound companions, V350 Sgr may also have two similar companions. While future studies may rule out one of these possible companions and hence remove the question of stability, the fact that half the stars in Table 7 are in this situation may reflect something about star formation. One way to have a pair of companions at apparently similar separations but in a stable configuration is that they are not coplanar, but have very different inclinations. In summary, RV Sco, Y Car, and V350 Sgr may provide a clue to additional complexity in the formation processes.

The population of triple systems can have important effects on the evolution of the systems, such as in the Kozai–Lidov mechanism (Naoz 2016), as discussed in Section 6.10.

6.8. Detection Probability

The following example provides an indication of the completeness of the survey. For a typical distance in

Table 8
Typical Magnitude for Probable Detection

Spectral Type	M_V (mag)	V at 700 pc[a] (mag)
B9 V	+0.2	10.1
A3 V	+1.5	11.4
K0 V	+5.9	15.8

Note.
[a] Assuming $E(B - V) = 0.2$.

the WFC3 survey (700 pc) and a typical reddening $[E(B - V) = 0.20;$ Paper II], we estimate apparent magnitudes for a range of spectral types in Table 8; the M_V values are from Drilling & Landolt (2000). Using these magnitudes, the detection fraction from Figure 5 shows that nearly all the B9 and A3 companions would be detected outside 1″. Later spectral types (K0) are severely missing inside 1″6. Thus, for the example of 700 pc, essentially all early-type companions would be detected at separations larger than 700 au. For lower mass companions, as represented by the K0 star, they would be largely detected only outside 1100 au.

6.9. Companions Identified by Gaia

The Gaia spacecraft has provided new data to investigate multiple systems, particularly, to identify wide components from the outer regions of a star-forming cloud. This is also relevant to the question of whether there are stars formed at the same time that are neither gravitationally bound system members nor in a recognizable star cluster. In particular, studies have been made of proper motions to study orbits (Kervella et al. 2019a) and to identify wide companions (Kervella et al. 2019b).

Kervella et al. (2019a) have used the difference between proper motions from Gaia and Hipparcos to look for proper-motion anomalies resulting from orbital motion between the two epochs. Of the 70 stars in our WFC3 sample, they list data for 63, or 90%. (Of these 16, or 25%, had less-than-perfect Gaia data, often because the Cepheid is too bright.) The Gaia data showed proper-motion anomalies for 28 stars (44%) at the level of 2σ or greater, many of which are known spectroscopic binaries. We stress that this is only a first exploration of the Gaia results, which are expected to improve in the future. Specifically, other stars have indications of proper-motion anomalies, but at a lower significance level. As an example, S Mus is a well-known binary with an orbit, but does not meet the proper-motion-anomaly criterion.

6.9.1. Proper-motion Anomaly

Proper-motion Anomaly plus Orbit

Comparison of stars in the WFC3 survey and the Gaia proper-motion study is presented in Table 9 based on Tables A1, A2, and A3 in Kervella et al. (2019a), which lists the Cepheids that have proper-motion anomalies and orbits. Columns 2 and 3 in Table 9 contain the semimajor axis in mas and astronomical unit; Column 4 lists whether there is a resolved companion from Table 4 (Y); Column 5 whether a gravitationally bound (B) companion or a wide (W) comoving companion has been identified (see below); Columns 6 and 7 provide the separation for a gravitationally bound companion in astronomical units and mas; Column 8 the spectral type of the

companion; Columns 9 and 10 list the separation for a comoving companion (W), and its spectral type; and Column 11 reports whether the star is a cluster member (C) from Anderson et al. (2013). The semimajor axes are from Kervella et al. (2019a), Table 2. Because of the additional information from Gaia, particularly the individual parallaxes (which will be updated in DR3), they differ somewhat from the values in Table 6. Approximate spectral types have been inferred from the temperatures using the calibration of Pecaut & Mamajek (2013). (The symbol <M means cooler than M spectral types.) Two stars appear in Table 4 but not in either Table 9 or 10 (η Aql and BB Sgr). For η Aql the Gaia quality flags are poor, probably because it is very bright, so the information on a proper-motion anomaly is also poor. BB Sgr has no proper-motion anomaly and no wide companions.

When a spectroscopic orbit is known, the proper motions allow the orbit to be fully determined, including the inclination. By assuming a mass for the Cepheid, a mass for the secondary can be determined. In Table 9 we list the semimajor axes in astronomical units and milliarcseconds for stars with orbits (from Kervella et al. 2019a Table 2). Even when spectroscopic orbits are available, those shorter than 1000 days are considered preliminary (marked with a colon).

Proper-motion Anomaly without Orbit

In addition to the stars in Table 9, a number of stars were found to have a proper-motion anomaly that do not have an orbit: AV Cir, T Cru, X Cyg, β Dor R Mus, AP Pup, RV Sco, SZ Tau, LR TrA, AH Vel, and T Vul. However, for a number of these stars, the Gaia parameters are imperfect (X Cyg, β Dor, AP Pup, and T Vul).

It is likely that many of these have longer period orbits than stars for which orbits are known. This means that they are likely to sample the orbital period range of the WFC3 stars with resolved close companions (Table 3), making this range accessible by a second technique. Further information on these stars, for instance, from subsequent Gaia releases, is expected to provide new results for several sources, partly because the errors on the separations are large. For instance, X Cyg, SZ Tau, and T Vul (which have proper-motion anomalies) have accurate radial-velocity data that do not indicate orbital motion for periods shorter than 20 yr (Evans et al. 2015). On the other hand, T Vul has a hot companion, which must be in a wider binary orbit (Evans et al. 2013). T Cru and AH Vel are found by Bersier (2002) to be binaries. However, Gallenne et al. (2019) had difficulty identifying an orbital period from new velocity data. LR TrA shows orbital motion (Szabados et al. 2013). There is also some evidence of orbital velocity variation for R Mus, AP Pup, and RV Sco, as discussed by Szabados (1989). All the stars in this section (except for AV Cir and LR Tra) have been observed with IUE to search for hot companions. Only T Vul was found to have such a companion. The other stars had upper limits on spectral types in the early-A range, corresponding to companions less massive than $2.9–2.0\ M_\odot$. The whole group warrants further velocity observation; however, orbital periods of more than 20 yr are difficult to determine because they require a long time span of very accurate velocities.

There is a striking difference between system multiplicity of the proper-motion anomaly stars with and without orbits. In Table 9, the stars with orbits frequently have resolved companions from the WFC3 survey. In the group without orbits, only RV Sco has a WFC3 resolved companion.

Table 9
System Information from Gaia: PM Anomaly

	Sep (mas)	Sep (au)	Res Comp	Wide Comp	B Sep (au)	B Sep (mas)	SpTy	W Sep (au)	SpTy	Clust[a]
PM Anomaly: Orbits										
U Aql	5.64	20.47	Y							
FF Aql	4.47	8.22	Y							
V496 Aql	3.83	3.72								
RX Cam	4.21	3.41								
Y Car	3.73:	2.57:	Y	W				32300	K6 V	
SU Cas	1.65:	3.54:								
δ Cep	5.85	19.86		B	10800	40740	B7-8 III-IV +F0 V			
AX Cir	14.66	26.00	Y	B, W	42500	81490	M3.5 V	23000	M3 V	
SU Cyg	2.73:	3.27:		W				34400	K6 V	C
V1334 Cyg	6.18	7.29		W				43700	<M	
S Nor	8.87	9.67	Y	W				41100	K3 V	C
				W				38800	…	
S Sge	3.08:	2.07:								
X Sgr	2.40:	8.32:								
AW Per	27.22	29.15		B	8400	10270	K3.5 V			
V350 Sgr	5.16	5.24	Y	B	26200	29850	A2 V			
				B	30600	34920	K4.5 V			
V636 Sco	4.59	4.61								
U Vul	7.15	7.74	Y							

Notes. B Sep: separation for gravitationally bound companions. W Sep: separation for comoving companions.
[a] From Anderson et al. (2013).

Table 10
System Information from Gaia: Bound and Comoving Companion Candidates

	Res Comp	Wide Comp	B Sep (au)	B Sep (mas)	SpTy	W Sep (au)	SpTy	Clust[a]
No PM Anomaly								
V659 Cen[b]	Y	B	48300	62220	M3 V			
R Cru[b]	Y	B	6600	7700	G8 V			
Y Sgr[b]		W				33300	< M	C
		W				44300	…	
BP Cir		B	39000	66300	M2 V	48700	M9 V	
						33500	M3 V	
						29100	M2 V	
Y Oph		W				44000	K4 V	
U Sgr		B	43100	71990	A0 IV-V	40000	M0 V	C
		B	46100	76960	A0 V	21200	K7 V	
V950 Sco		B	15000	16070	G1 V	15800	G2 V	
						27300	K3 V	
R TrA		W				32600	K1 V	

Notes. B Sep: separation for gravitationally bound companions. W Sep: separation for comoving companions.
[a] From Anderson et al. (2013).
[b] Gaia quality parameters are imperfect.

Furthrmore, stars with orbits frequently have a Gaia companion either bound or comoving. None of the stars without orbits have these companions. Only X Cyg is identified as a cluster member by Anderson et al. (2013).

No Proper-motion Anomaly

In addition to the stars with a proper-motion anomaly (Table 9 with orbits, and those without a known orbit), a number of stars in the WFC3 sample showed no proper-motion anomaly in the Gaia analysis. In the case of η Aql, RT Aur, *l* Car, V659 Cen, ζ Gem, T Mon, S Mus, W Sgr, Y Sgr, and X Vul the Gaia astrometry in DR2 has large uncertainties, often because the stars are bright. The following stars have good astrometry solutions, but no proper-motion anomalies: TT Aql, V636 Cas, V Cen, V737 Cen, IR Cep, S Cru, BG Cru, DT Cyg, W Gem, BF Oph, V440 Per, RS Pup, MY Pup, BB Sgr, V482 Sco, S TrA, V Vel, and SV Vul.

6.9.2. WB and Comoving Companions

In addition to the proper-motion anomalies, Kervella et al. (2019b) have used Gaia data to identify more widely separated

Table 11
Summary: Separations for Systems with Resolved Companions

	Sep SB (au)	Sep Res (au)	B Sep (au)	SpTy	W Sep (au)	SpTy	Other (au)	Clust[a]
Close								
	Table 6	Table 6	Tables 9/10		Tables 9/10		Table 6	
R Cru	3:	1580	6600	G8 V				
U Aql	6.2	981					66	
U Vul	7.1	822						
S Nor	8.87	819			41100	K3 V	13300	C
					38800	…		
V659 Cen	3:	452	48300	M3 V				
η Aql	3.9:	191						
AX Cir	15.4	158	42500	M3.5 V	23000	M3 V		
	15.4							
Wide								
	Table 7	Table 7	Tables 9/10		Tables 9/10		Table 7	
AP Sgr	12:	5320						
Y Car	3.6	3820			32300	K6 V		
		alt 4700						
RV Sco	14:	4520						
		alt 2710						
V350 Sgr	2.7	2780	26200	A2 V				
			alt 30600	K4.5 V				
BB Sgr		2740						C
FF Aql	4.5	2520						

Notes. B Sep: separation for gravitationally bound companions. W Sep: separation for comoving companions. alt: alternate: not both dynamically stable.
[a] From Anderson et al. (2013).

companions. Candidates are selected because the companions and Cepheids have similar parallaxes, small differential tangential velocities, and a small projected linear separation. (The list is drawn from Table 1 in Kervella et al. 2019b for companions rated likely on the basis of visual inspection.) They further divide the candidates into gravitationally bound companions and unbound but comoving companions based on differential tangential velocities.

These companions are added to the entries in Table 9 when the Cepheids also have proper-motion anomalies, or are listed in Table 10 when they have no proper-motion anomalies. The top three entries in Table 10 (V659 Cen, R Cru, and Y Sgr) have imperfect Gaia quality parameters, so their status might change in the DR3 release. In Table 10, V659 Cen and R Cru have spectroscopic-binary companions, as discussed previously. BP Cir also shows orbital motion (R. I. Anderson et al. 2020, in preparation). As can be seen in Table 9, few of the Cepheids with proper-motion anomalies have *WC* companions. This is also true of the whole sample in Kervella et al. (2019b), where there are also distinctly fewer comoving companions than bound companions. (These wide companions would not, in general, have been in the field of our WFC3 survey.)

The comoving wide companions provide a first opportunity to consider companions formed at the same location as the intermediate-mass Cepheids, but independent of the binary-star formation process. This is a part of star formation that we have been unable to explore previously because of the difficulty of recognizing a single star as compared with a gravitationally bound companion or a cluster. It is possible that some of the gravitationally bound candidates may ultimately be reassigned

to the comoving group because the present analysis does not include radial-velocity information.

The occurrence of wide but gravitationally bound companions in Tables 9 and 10 varies markedly between the groups. In Table 9 (proper-motion anomaly with an orbit), 4 out of 17 systems (23%) have WB companions (B). The companions in this group have a range of spectral types from B through M, similar to the companion spectral types in Figure 6. Thus the companions do not appear to be dominated by field-star impostors. In Table 10 (no proper-motion anomaly but a wide companion or comoving star), five systems have a gravitationally bound companion. This makes a total of nine systems with a wide companion, or 13% of the whole WFC3 sample. The fact that the fraction of wide gravitationally bound companions is smaller in the whole WFC3 sample than in the subsample with proper-motion anomalies and orbits (Table 9) could be due to a different density in the star-forming environment.

For the comoving candidate companions, there is no particular reason to relate their occurrence to the details of the multiple systems. The comoving candidates, however, are heavily dominated by K and M dwarfs. This is similar to the color distribution of companions at more than 2000 au in Figure 7, indicating a larger fraction of impostor field stars, a change in properties of companions produced in star formation, or a dynamical evolution in multiple systems pushing smaller members outward.

We summarize the results for the Cepheids in the WFC3 study with resolved close and resolved wide companions in Table 11. The tables from which the separations are taken is indicated. Three stars (Y Car, RV Sco, and V350 Sgr) have two possible companions with roughly the same separation from the Cepheids, making it dynamically unlikely that both are

physical companions. We have marked one of the companions as an alternate (alt). As noted in Table 6 and Figure 8, stars with a close resolved companion also have an inner spectroscopic binary. It is also notable that three of the seven (or six, omitting S Nor) have wider gravitationally bound candidates, or 43 or 50%, much larger than the Cepheid sample as a whole (nine systems or 13%). Of the six resolved wide companion samples in Table 11 only one has a Gaia bound companion.

6.10. Multiplicity: Implications

Triple stars can form via two modes. First is an outside-in process, whereby core fragmentation on large scales initially produces the wide companions with $a_{out} > 100$ au, followed by disk fragmentation on smaller scales that forms the close inner binaries with $a_{in} < 100$ au (Moe & Di Stefano 2017; Tokovinin 2017). Second is an inside-out process, where two companions fragment within the same disk near $a_{in} \simeq a_{out} \simeq 10$ au in an initially unstable configuration, and then subsequent dynamical interactions throw one of the components (typically the least-massive) to larger separations or eject it entirely (Reipurth & Mikkola 2012; Moe & Kratter 2018). The Kozai–Lidov mechanism (Naoz 2016) also results in dynamical evolution of the system.

As discussed in Section 6.6, all companions to Cepheids with separations from 100 to 2000 au, and nearly all companions with separations between 2000 and 7000 au, are outer tertiaries to inner spectroscopic-binary companions with separations from 1 to 20 au. The strong link between outer tertiaries and inner binary companions to Cepheids suggests a causal link, e.g., the dynamical-unfolding scenario. Nearly all of the outer tertiary companions are less massive than the inner spectroscopic-binary companions, consistent with the triple-star dynamical-unfolding scenario. In this dynamical-unfolding scenario, the outer tertiaries are expected to be highly eccentric, which may be tested in the future with Gaia astrometry.

Nonetheless, correlation does not necessarily imply causation. The binary fraction of O-type (Sana et al. 2014) and early-B (Moe & Di Stefano 2017) stars is nearly 100% within $a < 100$ au, and therefore nearly all wide companions beyond $a > 100$ au to massive stars are outer tertiaries in hierarchical triples. Similarly, Evans et al. (2005) showed that triples are quite common among Cepheids, and again, Evans et al. (2015) found that 30% of Cepheids have companions for a between 1 and 20 au, probably because Cepheids began life as late-B stars. In addition, B stars in short-period orbits will have merged before the Cepheid stage, removing them from the binary statistics. The preponderance of Cepheids in hierarchical triples with a_{in} between 1 and 20 au and a_{out} between 100 and 7000 au could simply be due to the efficient formation of companions to massive stars via both disk fragmentation and core fragmentation on small and large scales, respectively. On the other hand, the estimates in Tables 6 and 7 show that the spectroscopic companions are within 20 au, the regime that was well studied in Evans et al. (2015). The binary fraction from that study is 30%. Thus, in Table 6, of the seven Cepheids with companions, two would be expected to have spectroscopic-binary companions, rather than all seven. Similarly, in Table 7, two of the seven stars would be expected to have companions in this range rather than six. In sum, 13 of these 14 stars have spectroscopic companions within 20 au where four are expected, strongly implying that the system structure (triples) is not produced by the standard outside-in process.

Wide companions that derive from core fragmentation have systematically lower masses than inner binary companions that come from disk fragmentation (Moe & Di Stefano 2017). This is the case for Tables 6 and 7. Our wide tertiaries are systematically less massive than the inner binaries, but are still top-heavy compared to random pairings from the IMF.

Although a significant majority of very wide companions to solar-type stars are tertiaries, Tokovinin (2017) argued that most derive from fragmentation of adjacent cores, not dynamical unfolding, and therefore there is no causal link between inner binaries and outer tertiaries. This is related to the possibility that some Cepheids are the remnants of dispersed clusters (Anderson & Riess 2018). The identification of wide binaries formed from separate but adjacent cores derives from the fact that beyond about 10,000 au, the number of companions increases strongly, beyond those presumably formed by core or disk fragmentation. Insight here comes from the Gaia wide companions. Wider companions from Gaia (Tables 9 and 10) from adjacent cores are expected to show some degree of correlation in component masses compared to independent cores (Tokovinin 2017). The frequency of these very wide companions rises steeply beyond about 10,000 au. Tables 9 and 10 show that 16 Cepheids have either bound or unbound Gaia companions, very similar to the 13 Cepheids with resolved companions in the WFC3 study. The most likely explanation is that the Gaia survey only extended to 50,000 au, where core/disk fragmentation stars are mixed with adjacent core stars. This may be an indication of the density of the formation environment (Deacon & Kraus 2020).

In reality, both an outside-in formation via the relatively independent processes of core fragmentation followed by disk fragmentation and an inside-out mode via dynamical unfolding likely contribute to our Cepheid triple sample. The Cepheid sample discussed here contributes to the sample of massive triples needed to fully compare the companion mass distributions to the two different models and determine which scenario is dominant. As indicated above, astrometric orbital solutions (or at least a sense of relative orbital motion) of the outer tertiaries will also help constrain their formation mechanism.

7. Summary of This Series of Papers

This paper completes the discussion of the series reporting results of our HST/WFC3 two-color search for resolved companions of 70 Galactic Cepheids. In the present paper we identified candidate stars lying at separations between 0″5 and 5″0, and present a list of the most probable companions. Our major results from the series are summarized here.

1. Detection of companions of bright Cepheids lying within 2″ requires sophisticated image processing. In our sample, seven Cepheids have companions within this range.

2. Discussion of the identifications, separations, and spectral types of the companions has been aided by Chandra observations of R Cru and S Mus, and also HST/STIS spectra of U Aql and AX Cir. We provide a discussion of components for these systems (R Cru, η Aql, S Nor, U Aql, U Vul, V659 Cen, and AX Cir).

3. The $(V - I)_0$–M_V CMD shows that the companions are fairly evenly distributed in mass (as opposed to being dominated by low-mass companions). However, this may be partly because low-mass companions are more difficult to discover within 1″ of the Cepheid. In contrast, companion candidates with wider separations are less massive than 1.5 $M_\odot$.

Cepheids with companions within 2″ with separations of a few hundred astronomical units comprise 10% of those in the survey.

4. It is particularly striking that companion candidates in the 0″5 to 2″0 range, corresponding to separations smaller than 2000 au, all have an inner binary system. This is in contrast with the typical fraction of Cepheids in spectroscopic binaries of 29% ± 8% found in a velocity sample. It is also clear that the resolved companion may be either more or less massive than the spectroscopic-binary companions.

5. Companions wider than 2″ also have an inner spectroscopic binary for all or most systems (Table 7 and Figure 9).

6. As discussed in Section 6.10, in a standard scenario, it seems more likely that the resolved companion is formed first in a core-collapse process, followed by the formation of the spectroscopic binary through disk fragmentation. In this scenario it is unlikely that the formation of the outer component can anticipate the formation of an inner binary. The most likely explanation that the resolved companion seems to require a spectroscopic binary is that that combination results from dynamical evolution, which can, of course, occur in triple systems. However, processes of outside-in formation, adjacent cores, and the dissolution of clusters may be involved in some cases.

7. In order to place the Cepheid multiple systems in context, we have also used Gaia results to incorporate proper-motion anomalies into orbits (Kervella et al. 2019a) and to identify wider companion candidates (gravitationally bound and comoving; Kervella et al. 2019b). The occurrence of wide companions is about 14%.

This paper focuses on Cepheids with companions at separations from approximately 100 au to several thousand astronomical units. This group has several characteristics relevant to the formation of multiple stellar systems. All have an inner (spectroscopic) binary. The distribution of companion spectral types (temperatures) or masses is distinctly different for companions within about 2000 au and those at wider separations (Figure 7). As discussed in item 6 above, the properties of companions provide clues to the formation and evolution of the systems. Thus, although the properties of companions in multiple systems are difficult to obtain, this group warrants further observation.

Facility: HST (WFC3) Chandra.

Software: DrizzlePac (Hack et al. 2013), Astropy (The Astropy Collaboration 2013), DAOPHOT (Stetson 1987), Sherpa (Freeman et al. 2001; Doe et al. 2007) Photutils (Bradley et al. 2019), and IRAF (Tody 1986, 1993).

Appendix A
Candidate Companions with Separations between 2″ and 5″: Resolved Wide Companions

The images and CMDs for companion candidates with separations between 2″ and 5″, discussed in Section 3, are presented in this appendix (Figures 10–15). The CMDs include stars from the full WFC3 images, but the companion candidates indicated by arrows are only from the 2″ to 5″ region.

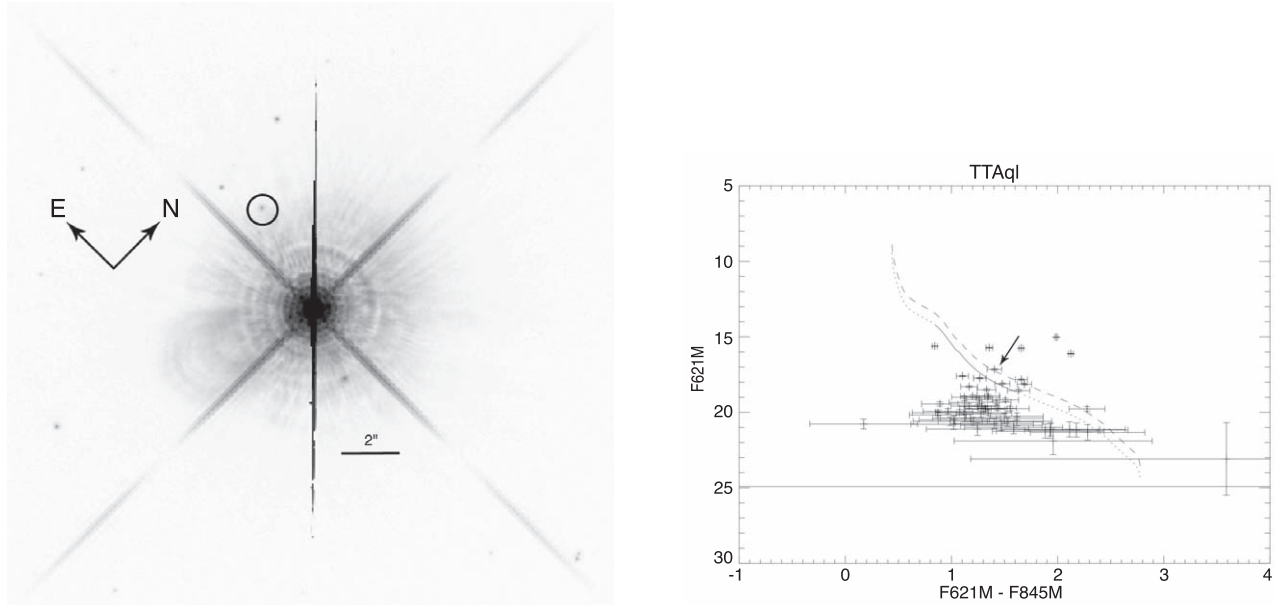**Figure 10.** (left) The inner portion of the F845M WFC3 image of TT Aql. The possible companion is circled. A log scale is used, and 2″ is indicated by the bar. (right) The CMD from the F845M and F621M WFC3 images. The lower line is the ZAMS at the distance and with the reddening of the Cepheid. The solid portion is the spectral region of F2 to K7; dotted parts are the extension to other spectral types. The dashed line is 0.75 mag brighter to include binaries. The arrow perpendicular to the ZAMS indicates the possible companion. Other stars within this band are more widely separated from the Cepheid; they were discussed in Paper II.
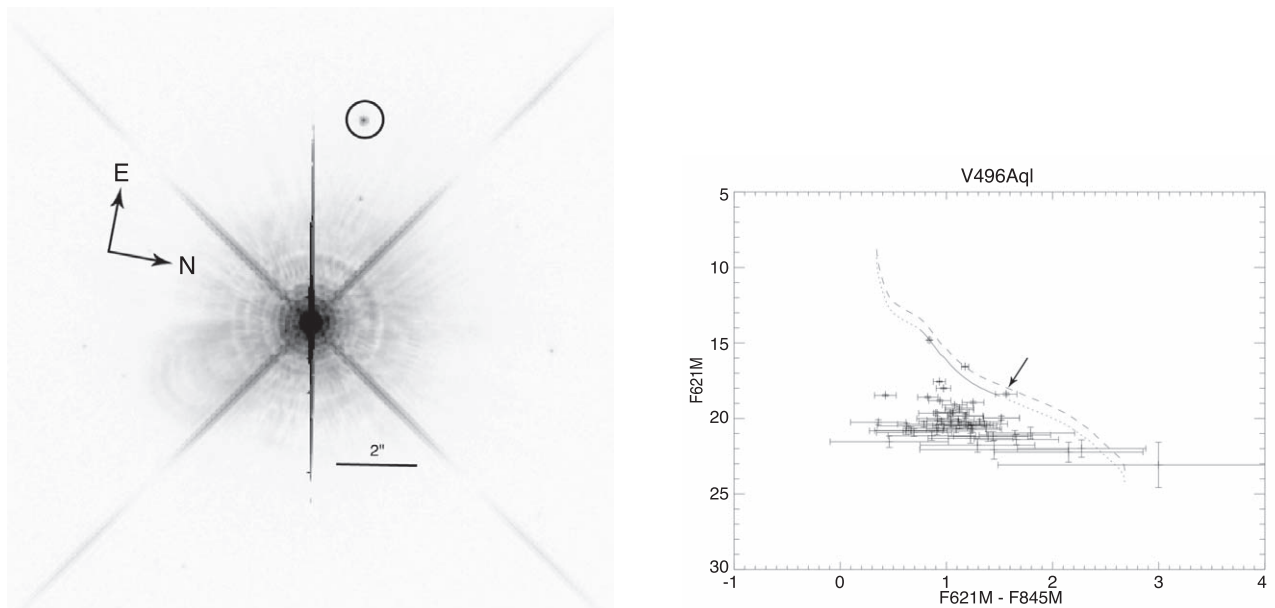
Figure 11. (left) The inner portion of the F845M WFC3 image of V496 Aql. The possible companion is circled. A log scale is used, and 2″ is indicated by the bar. (right) The CMD from the F845M and F621M WFC3 images for V496 Aql. Symbols are the same as for Figure 10.
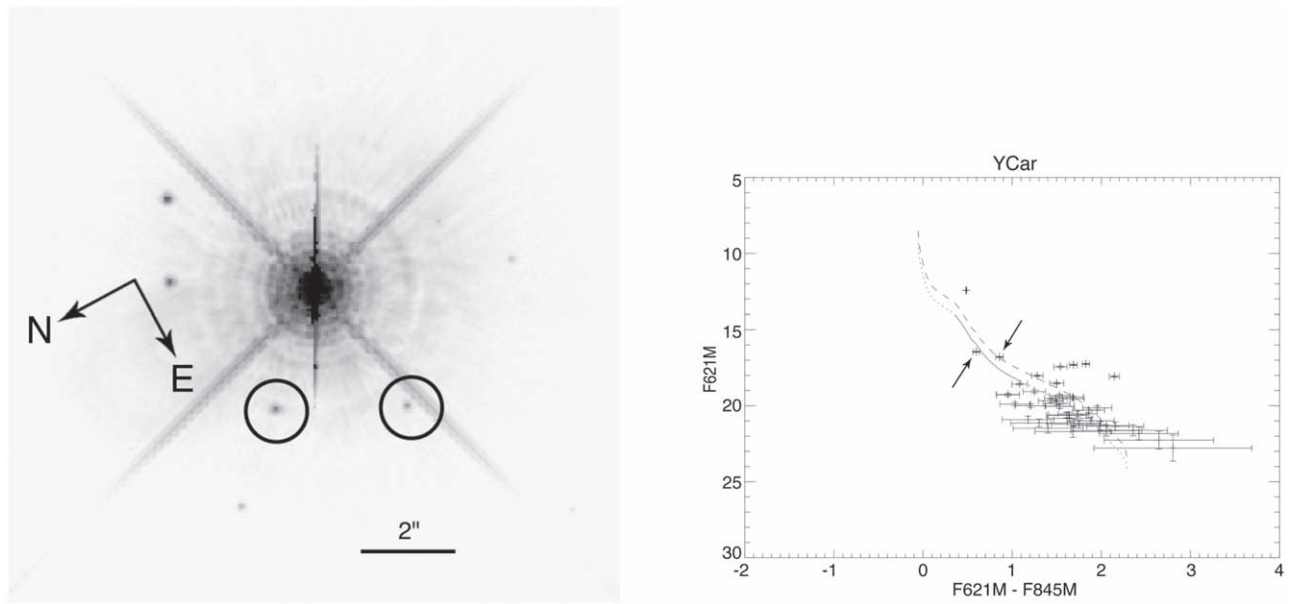
Figure 12. (left) The inner portion of the F845M WFC3 image of Y Car. The possible companions are circled. A log scale is used, and 2″ is indicated by the bar. (right) The CMD from the F845M and F621M WFC3 images for Y Car. Symbols are the same as for Figure 10.
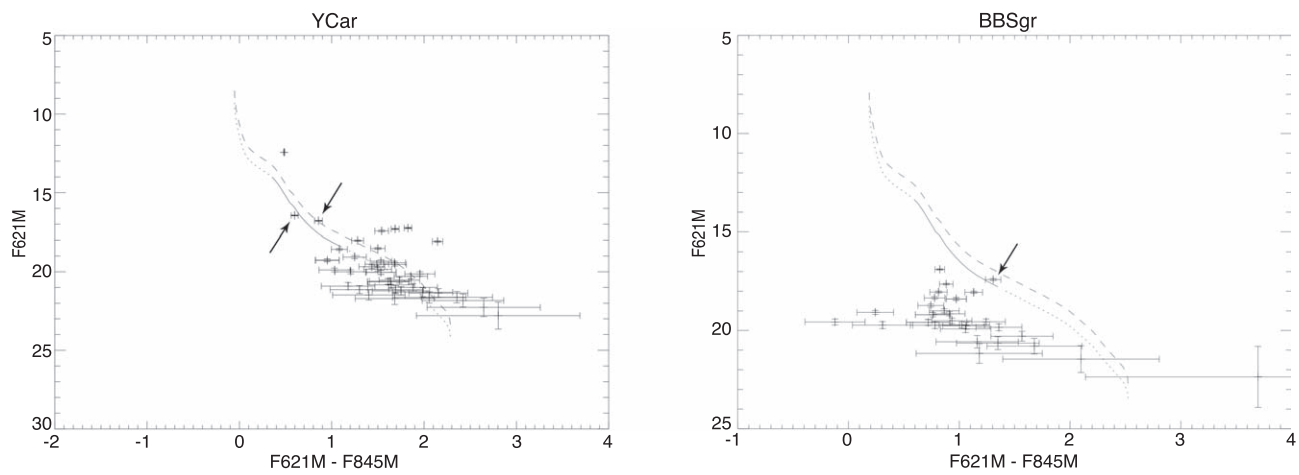
Figure 13. (left) The inner portion of the F845M WFC3 image of BB Sgr. The possible companion is circled. A log scale is used, and 2″ is indicated by the bar. (right) The CMD from the F845M and F621M WFC3 images for BB Sgr. Symbols are the same as for Figure 10.
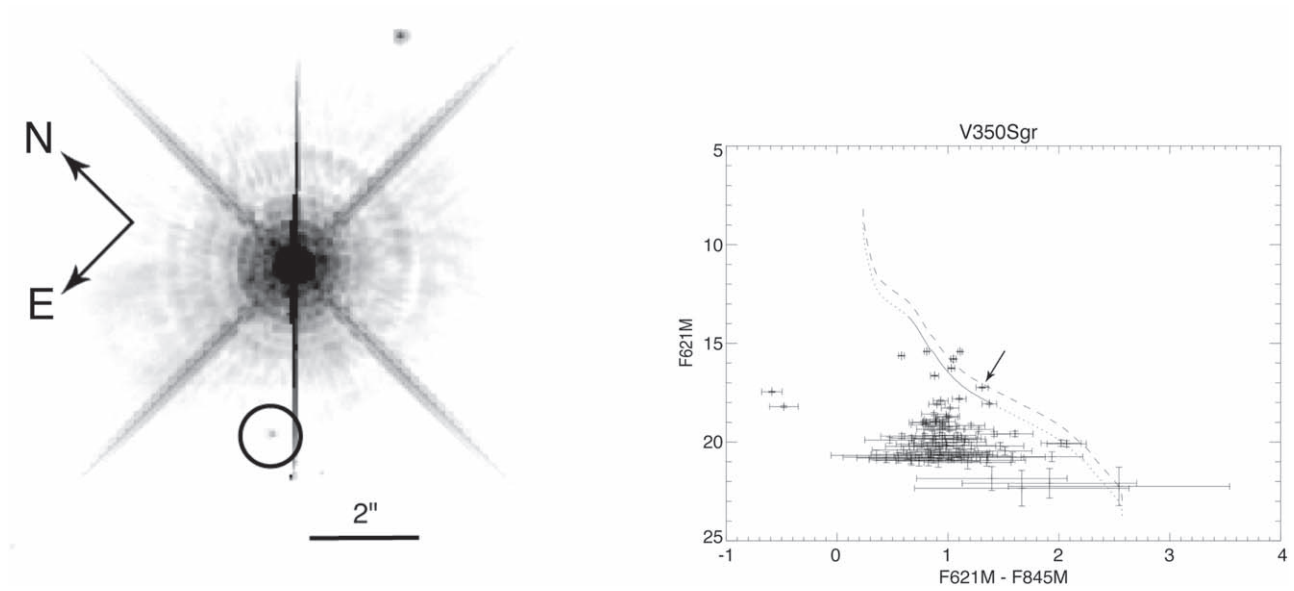
Figure 14. (left) The inner portion of the F845M WFC3 image of V350 Sgr. The possible companion is circled. A log scale is used, and 2″ is indicated by the bar. (right) The CMD from the F845M and F621M WFC3 images for V350 Sgr. Symbols are the same as for Figure 10.
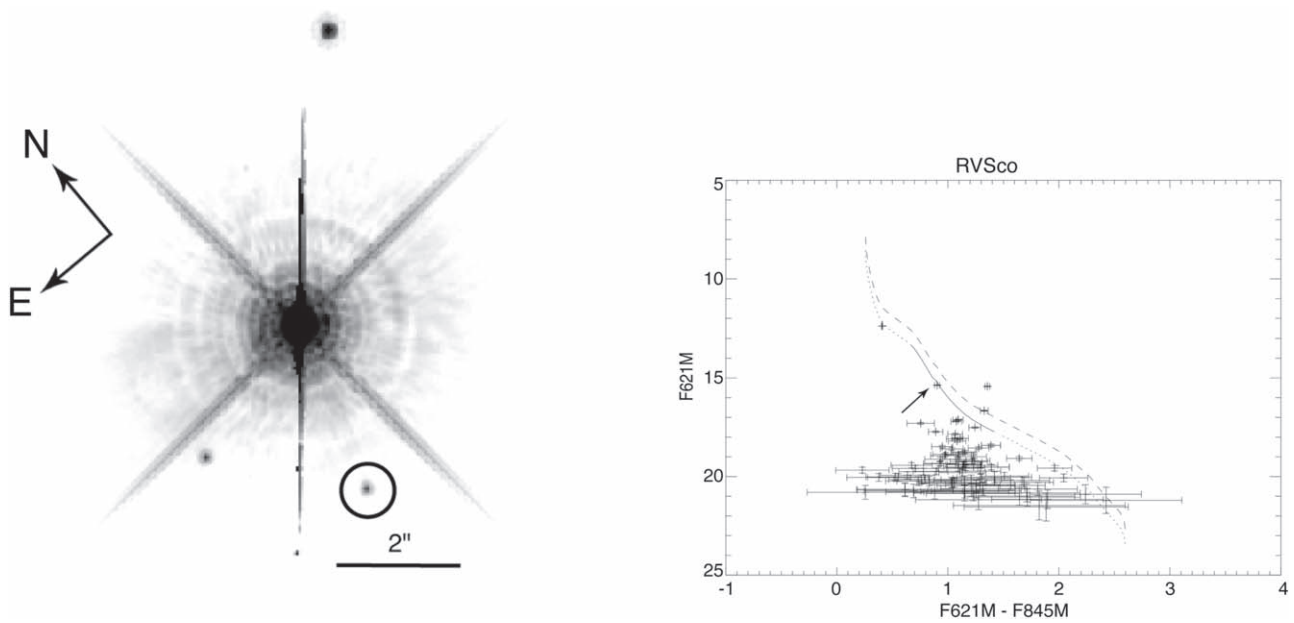
Figure 15. (left) The inner portion of the F845M WFC3 image of RV Sco. The possible companion is circled. A log scale is used, and 2″ is indicated by the bar. (right) The CMD from the F845M and F621M WFC3 images for RV Sco. Symbols are the same as for Figure 10.

Appendix B
Candidate Companions within 2″: Resolved Close Companions

The HST images for companion candidates within 2″, discussed in Section 4.3.2, are presented in this appendix (Figures 16–24) both before and after PSF correction.
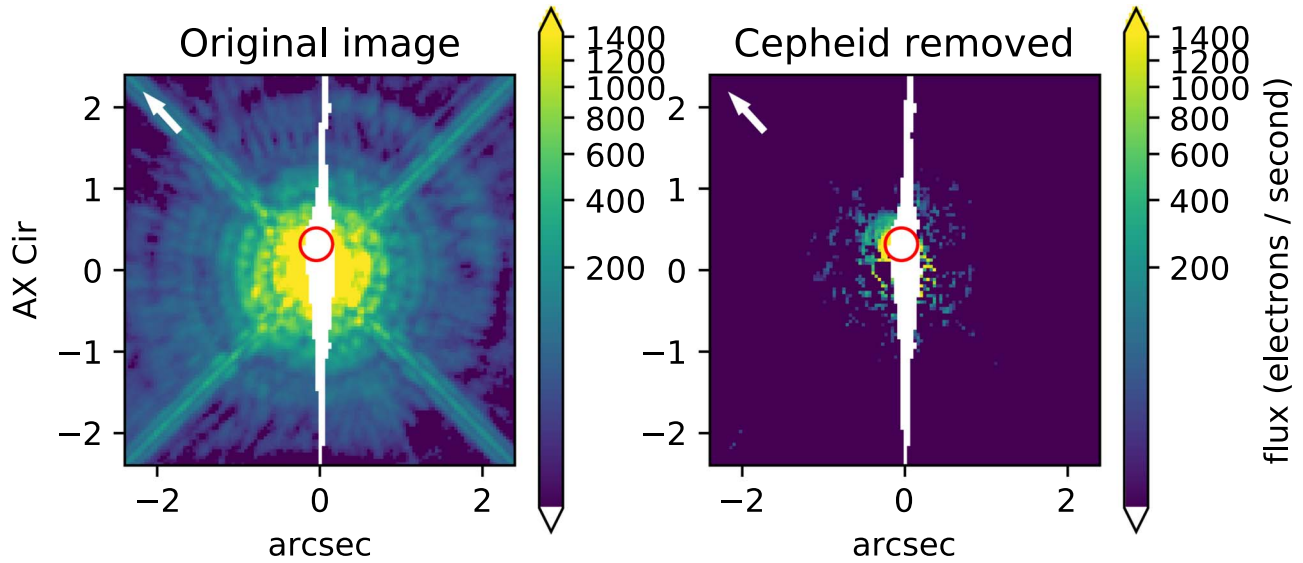
Figure 16. Image of AX Cir in the F845M band. The image is displayed in the same way as for Figure 3 (η Aql). Left: original image. Right: after LOCI subtraction.
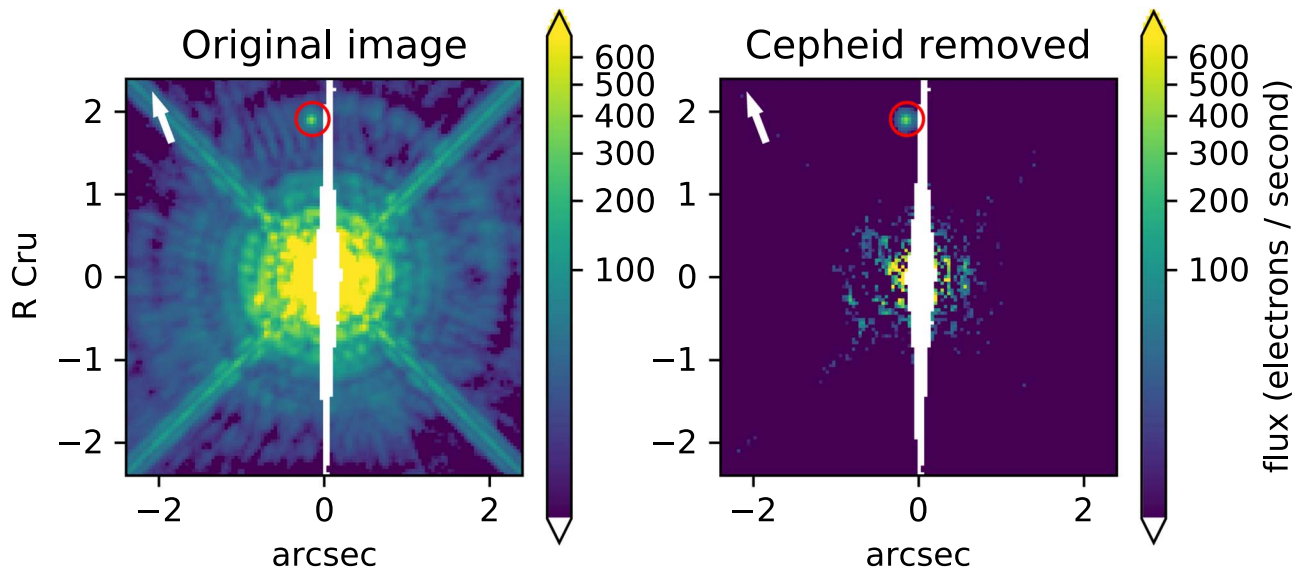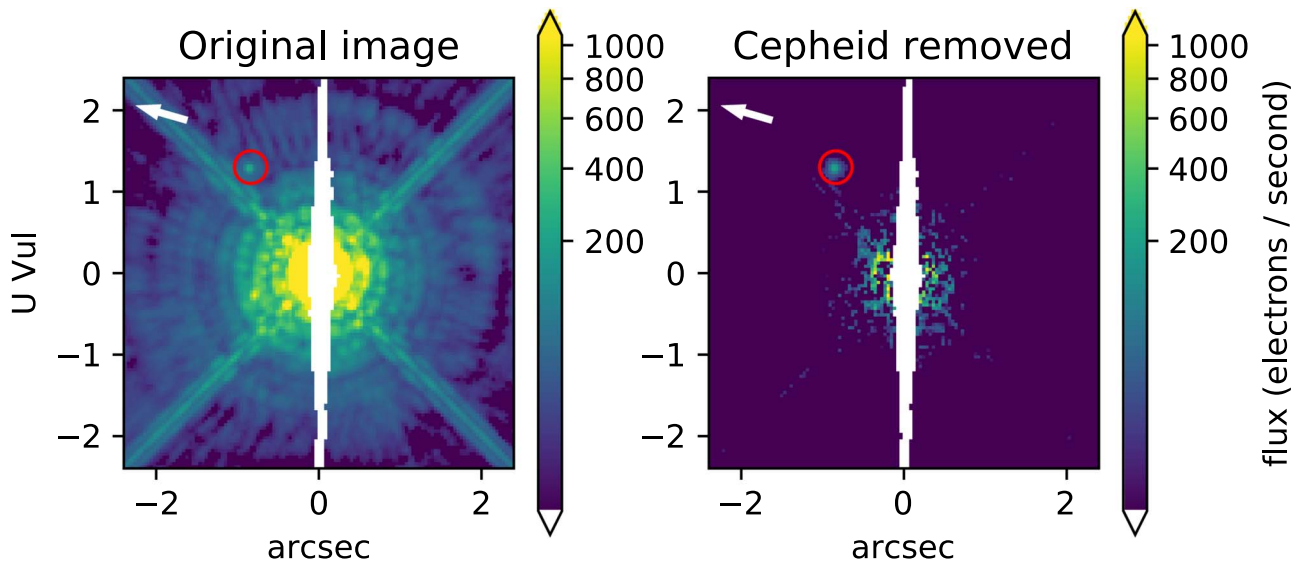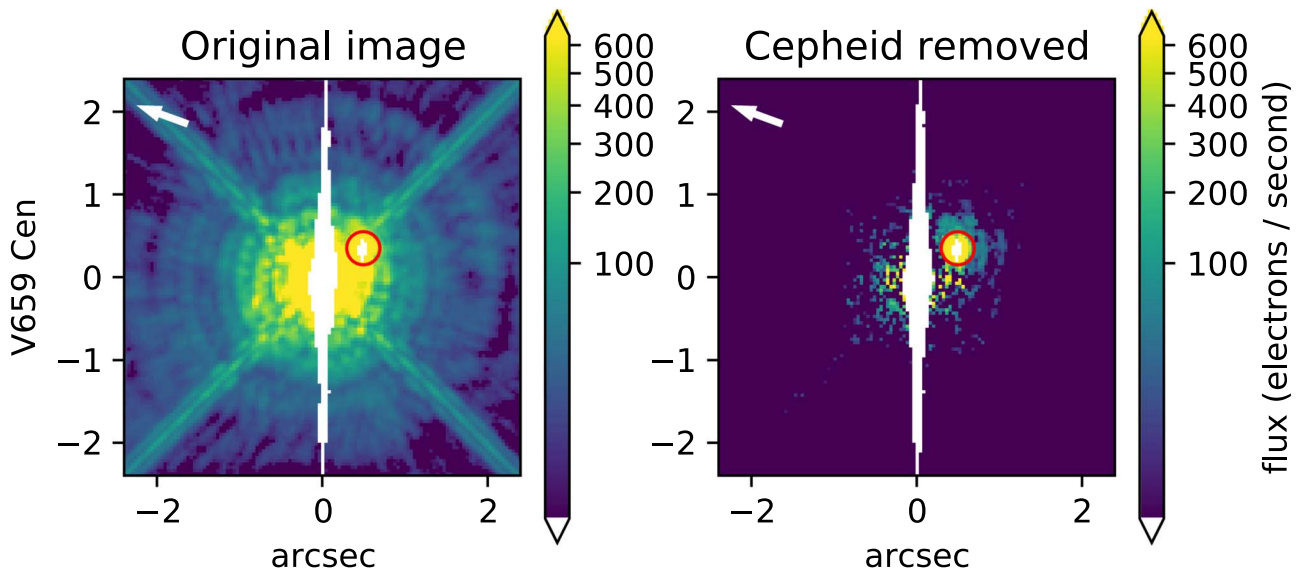

Figure 17. Image of R Cru in the F845M band. The image is displayed in the same way as for Figure 3 (η Aql). Left: original image. Right: after LOCI subtraction.
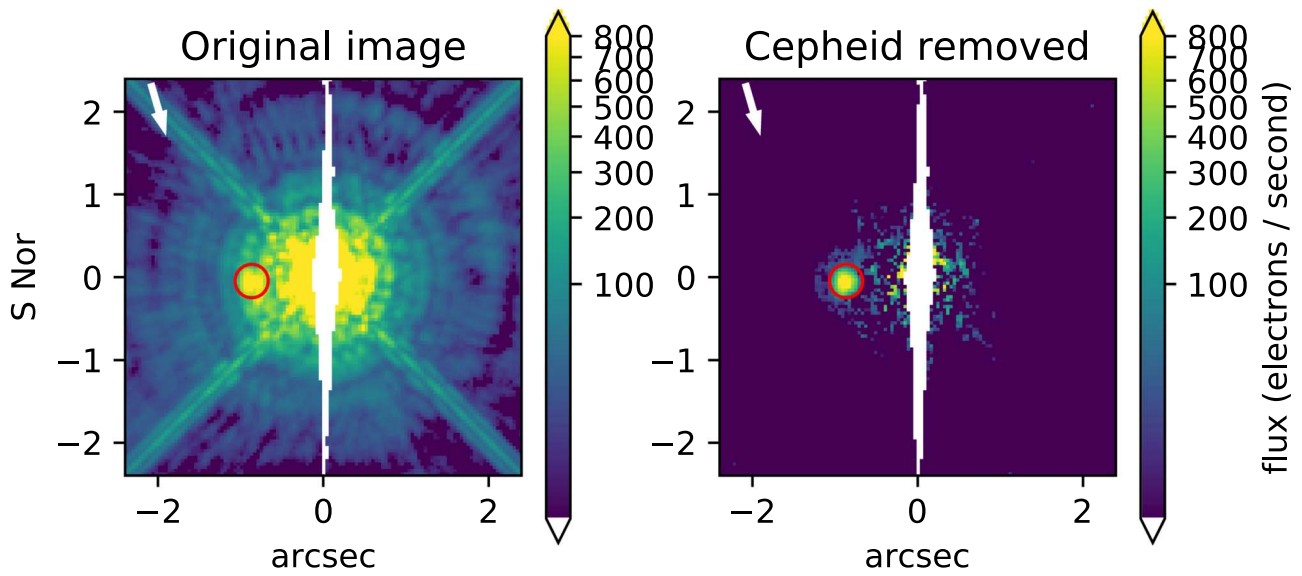
Figure 18. Image of S Nor in the F845M band. The image is displayed in the same way as for Figure 3 (η Aql). Left: original image. Right: after LOCI subtraction.
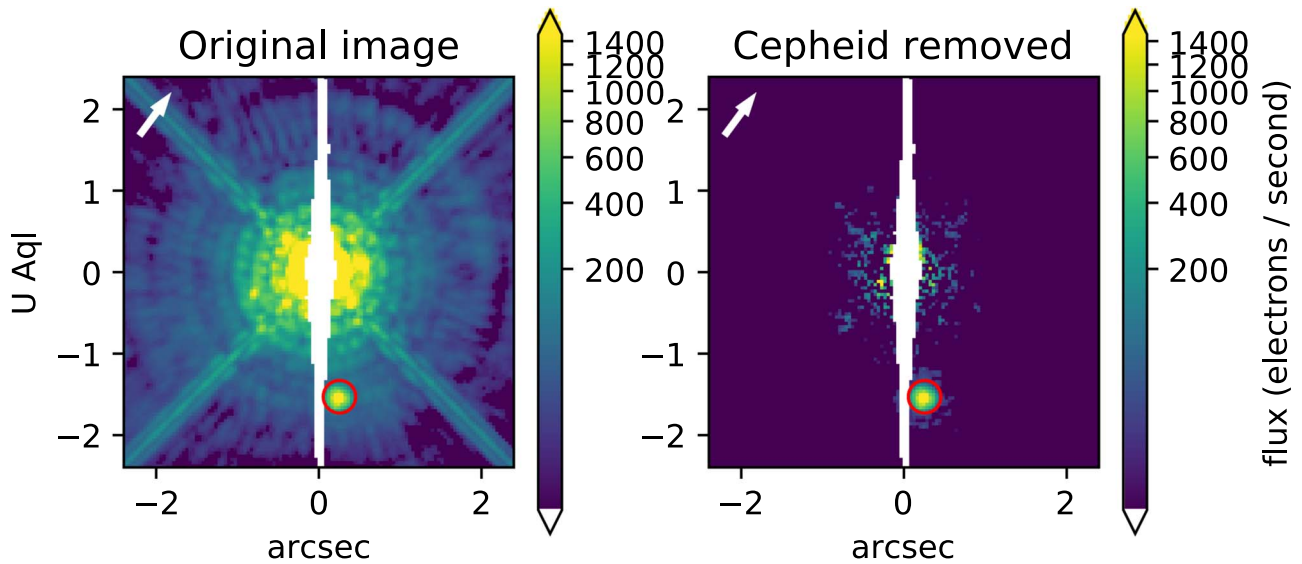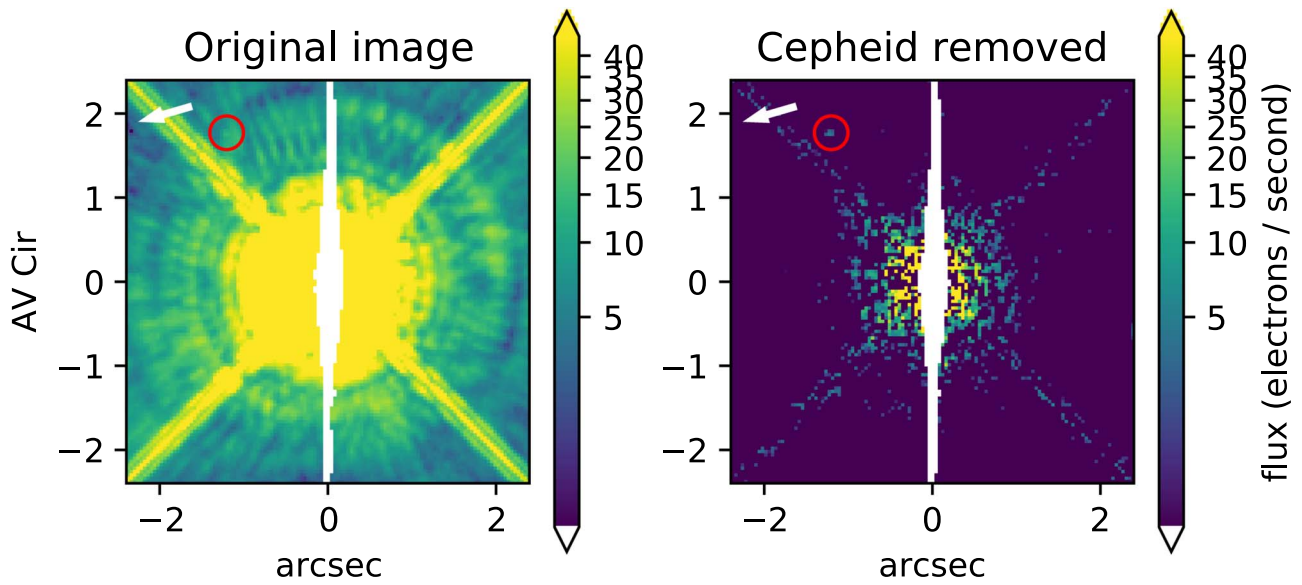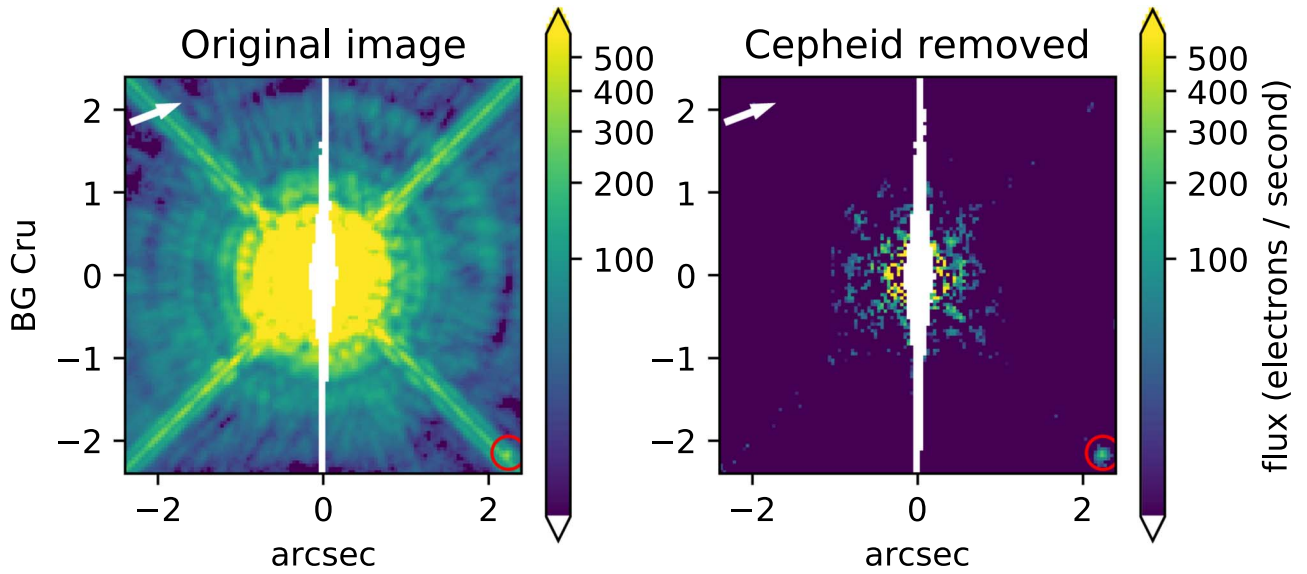

Figure 19. Image of U Aql in the F845M band. The image is displayed in the same way as for Figure 3 (η Aql). Left: original image. Right: after LOCI subtraction.

Figure 20. Image of U Vul in the F845M band. The image is displayed in the same way as for Figure 3 (η Aql). Left: original image. Right: after LOCI subtraction.
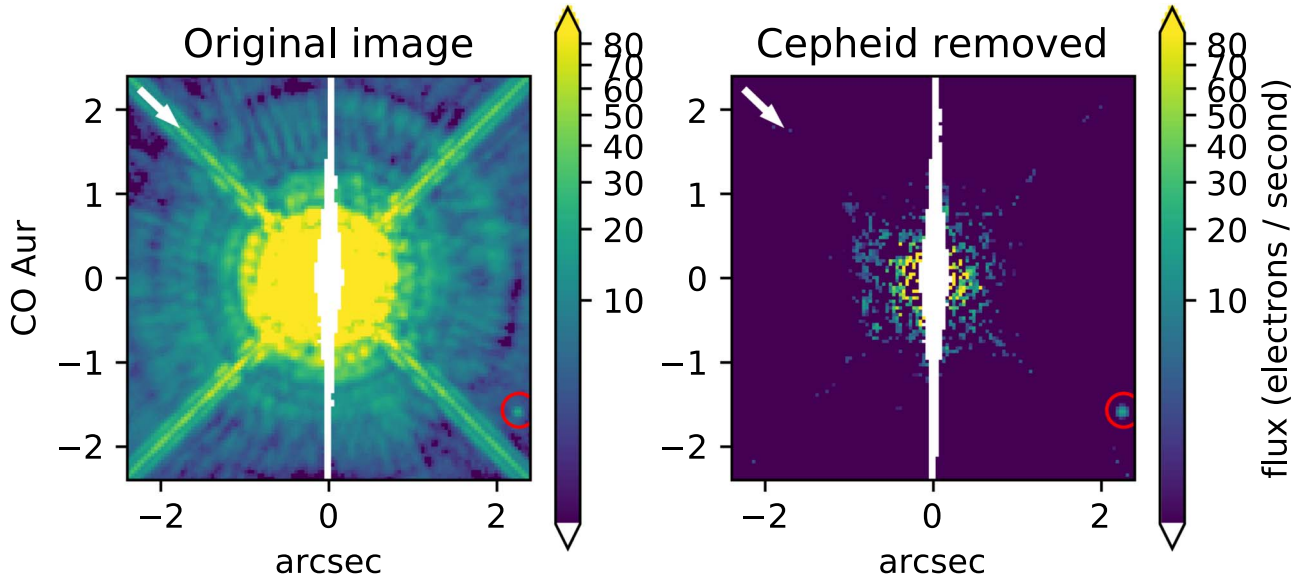
Figure 21. Image of V659 Cen in the F845M band. The image is displayed in the same way as for Figure 3 (η Aql). Left: original image. Right: after LOCI subtraction.

Figure 22. Image of AV Cir in the F845M band. The image is displayed in the same way as for Figure 3 (η Aql). Left: original image. Right: after LOCI subtraction.

Figure 23. Image of BG Cru in the F845M band. The image is displayed in the same way as for Figure 3 (η Aql). Left: original image. Right: after LOCI subtraction.

Figure 24. Image of CO Aur in the F845M band. The image is displayed in the same way as for Figure 3 (η Aql). Left: original image. Right: after LOCI subtraction.

Appendix C
Chandra Observations

The goal of this paper is to identify resolved companions in the Cepheid HST snapshot survey and to examine the properties of members of the systems they belong to. As discussed in Paper IV, X-ray observations are an excellent way to distinguish between an X-ray-active star young enough to be a physical Cepheid companion, and an old field star without appreciable X-ray activity. Since Paper IV, we have added Chandra observations for two stars that add to the understanding of system parameters. The two systems were found to be X-ray sources in Paper IV: R Cru (Table 2) and S Mus. Among the XMM targets, they had X-ray detections at approximately the position of the Cepheid, but with a possible companion that was not resolved from the Cepheid in the XMM images. We followed up these detections with Chandra observations to identify the source of the X-rays, using the

Table 12
Chandra Observations

Star	OBSID	JD −2,400,000	Exp. (ks)
S Mus	17740	57,388.068	5.0
R Cru	17741	57,578.170	14.9

higher resolution of Chandra. S Mus and R Cru were observed with the Advanced CCD Imaging Spectrometer (ACIS) using the four "I" CCD chips. Details are provided in Table 12.

C.1. R Cru

The HST and XMM images are shown in Figure 25, with the locations of the Cepheid and the possible optical companions
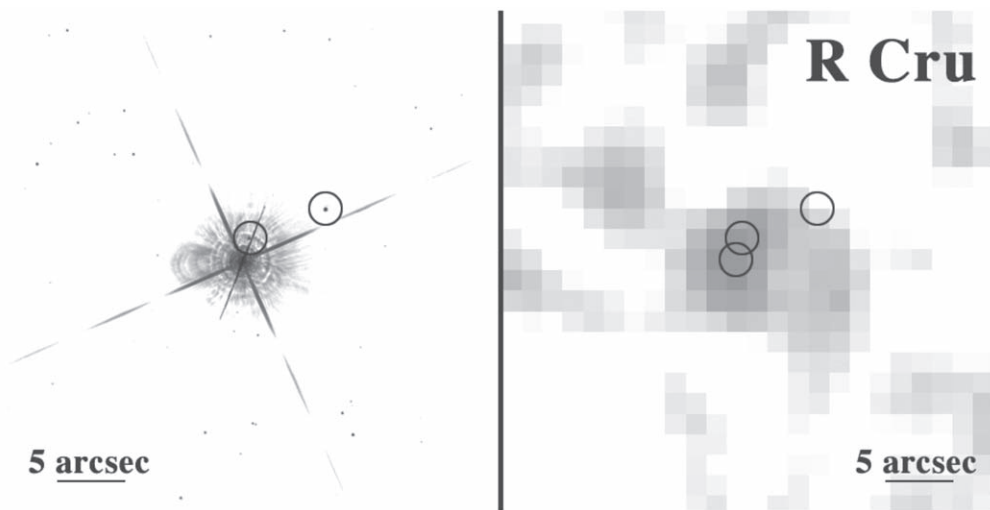
Figure 25. Possible companions of R Cru. Left: HST WFC3 *I*-band image of R Cru. Possible companions are circled. The stretch is logarithmic to emphasize faint features. Right: XMM image, again with circles indicating locations of the Cepheid and its two possible companions (including a small correction derived from the X-ray positions of 2MASS sources). The orientation of both panels is the same: north is up, and east is to the left.
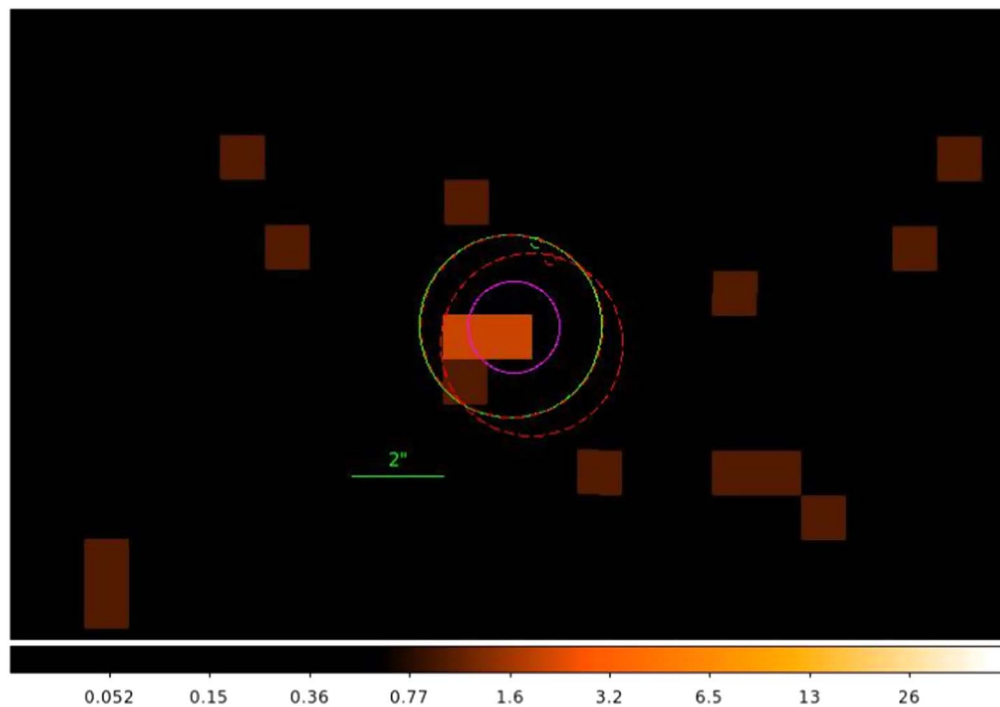

Figure 26. The center of the Chandra image of R Cru, showing the Cepheid and the closer companion. The orientation is the same as in Figure 25. The bright red rectangle is the location of the Chandra source. The circles are as follows: green: $2''$ radius centered on the position of the Cepheid from SIMBAD (including proper motion); red: the same radius centered on the Cepheid in the HST image; and magenta: $1''$ radius within the green position of the Cepheid. The position of the companion from the HST image is shown by the very small red and green circles (about 1 o'clock) corresponding to the positions of the Cepheid in those colors. The image is a log stretch.

circled. Either of the possible companions could be the source of the X-rays in the XMM image (although the closer one is more likely).

The Chandra image of R Cru is shown in Figure 26, which compares the location of the X-ray source to that of the Cepheid and the possible close companion (including a small shift to align the Cepheid in the HST image with its coordinates from SIMBAD). The shape of the X-ray source based on a relatively weak detection has some uncertainty, but it is closer to the Cepheid than to the possible close companion.

Are the X-rays from the Cepheid itself? We now have a pattern to X-ray activity in Cepheids (Engle et al. 2017): it is relatively constant at about $\log L_X = 28.8$ erg s^{-1} for most of the pulsation cycle, but has a burst of X-rays just after maximum radius (approximately phase 0.5). The X-ray flux from XMM for R Cru ($\log L_X = 29.8$ erg s^{-1}; Paper IV) is higher than the quiescent level. The phase of the Chandra observation is 0.94 (using the period 5.825701^d and the epoch of maximum light of JD 2455172.5100 from Usenko et al. 2014), not the phase of X-ray maximum. Thus the X-ray flux is
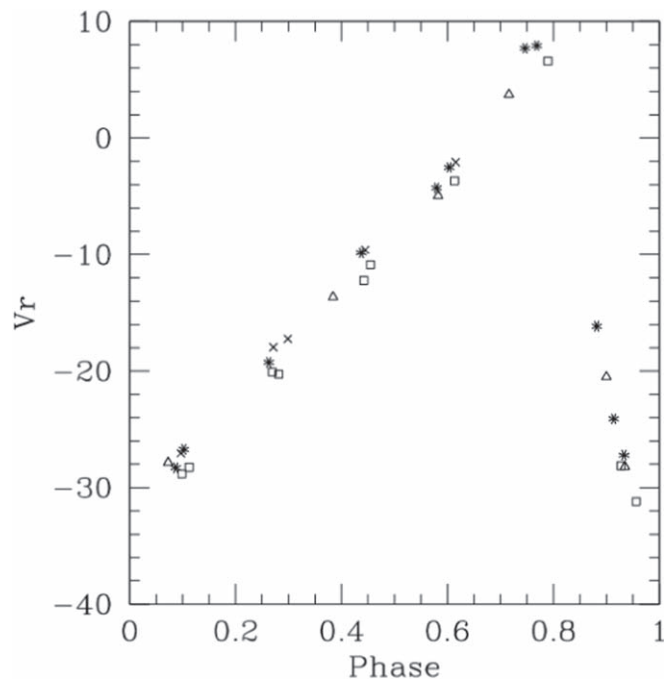
Figure 27. CORAVEL radial velocities of R Cru. The sequence of the four seasons of observations from first to last is crosses, asterisks, squares, and triangles (see text). The displacement of the squares from the crosses and asterisks is particularly apparent. Velocities are in km s^{-1}.
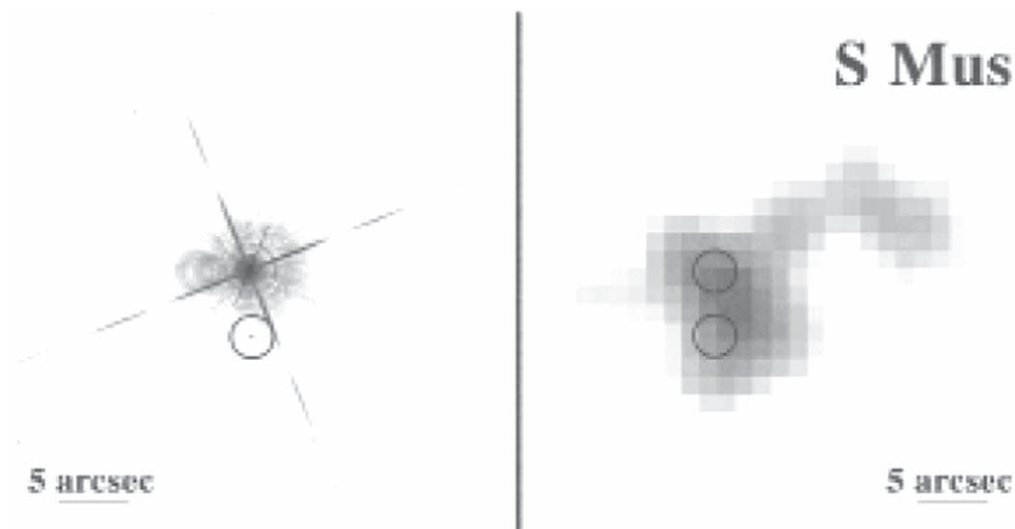

Figure 28. Possible companion of S Mus. Left: The HST WFC3 *I*-band image of S Mus. The possible companion is circled. The scale is logarithmic to emphasize faint features. Right: The XMM image, again with circles indicating the locations of the Cepheid and the possible companion (including a small correction derived from the X-ray positions of 2MASS sources). The orientation of both figures is the same, N is up and E to the left.

higher than expected for the Cepheid, particularly at a phase other than maximum radius.

There is, however, another possibility. R Cru was observed with the CORAVEL radial-velocity spectrograph for four seasons, approximately 1996 July, and 1997 March, July, and December (Bersier et al. 1994). The results are shown in Figure 27, with different symbols for each season. The velocities for the third season (and to some extent, the fourth) fall below the first two, particularly considering that a typical error for the velocities is 0.33 km s^{-1}. This indicates a systemic velocity change within a year, presumably due to orbital motion. This implies that there is a second companion candidate in a close orbit, which would be unresolved from

the Cepheid in the Chandra observation. An orbit with a period of almost a year corresponds to a separation near one astronomical unit.

There is one further piece of information that gives insight into the R Cru system. It was observed with IUE (Evans 1992a), with the result that any companion must have a later spectral type than A2, corresponding to a mass lower than 2.5 $M_\odot$.

To summarize companion possibilities for R Cru, there are two reasonably close companions, one at a separation of 1580 au (Table 4), and the spectroscopic-binary companion (Figure 27) at approximately 1 au. Note that these two would be dynamically compatible. The Chandra observation in
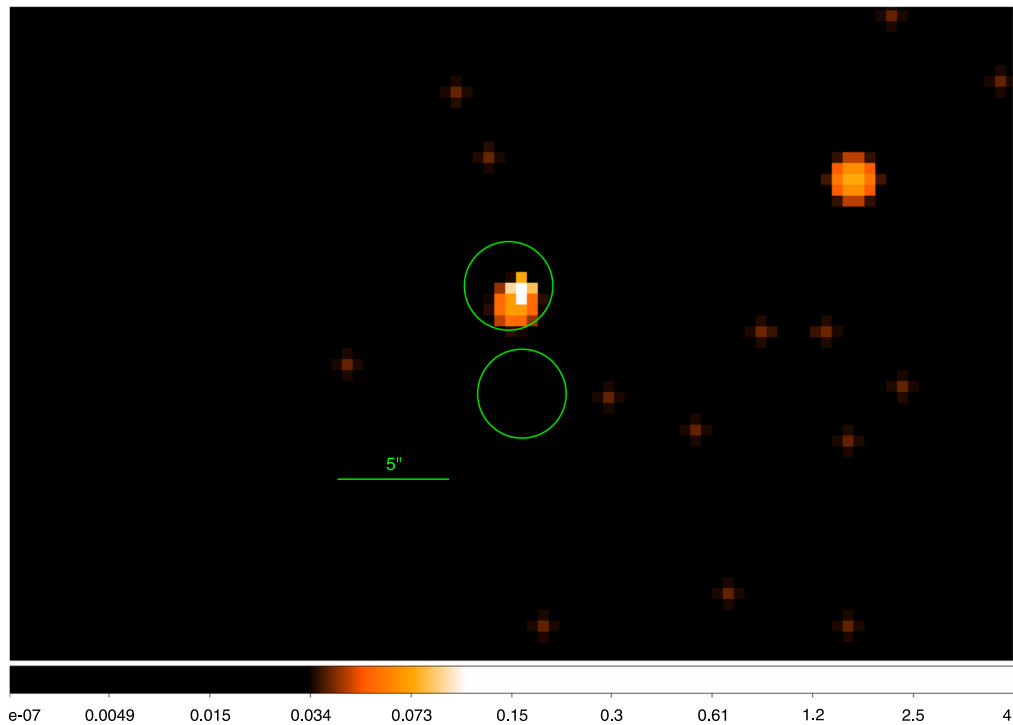
Figure 29. The center of the Chandra image of S Mus. The orientation is the same as Figure 28. The two circles ($2''$ radius) show the positions of the Cepheid and the possible companion in Figure 28. The image counts are on a log scale and have been mildly adaptively smoothed.

Figure 26 provides an indication favoring the closer companion, but this is tentative. However, Gaia data (Kervella et al. 2019b) provide additional evidence that the candidate at 1580 au is a physical companion, as discussed in Appendix D. Therefore we continue to include it in Table 4. The IUE observation shows that any companion is only about half as massive as the Cepheid (or less).

C.2. S Mus

The HST and XMM images are shown in Figure 28, with the locations of the Cepheid and the possible companion circled. Figure 29 shows the Chandra image with the same two locations overlaid. It has been mildly smoothed with the *CIAO* tool smooth.

The Chandra image rules out the $5''\!.2$ (4540 au) companion as young, and hence it is not a physical companion of the Cepheid S Mus. The Cepheid is a member of a spectroscopic-binary system with a period of 505 days ($a \sin i = 2.8$ au; Paper I). The companion is the hottest known Cepheid companion: B3 V (Evans et al. 2006). Stars this hot produce X-rays through wind shocks (Harnden et al. 1979), typically with $L_x/L_{bol} = 10^{-7}$. When M_{bol} is used for a B3 star of -4.0 (Drilling & Landolt 2000), the luminosity is 1.2×10^{37} erg s^{-1}. Thus the X-ray luminosity of $\log L_X = 30.46$ (Paper IV) is close to the expected ratio for a hot star. The phase of the Chandra observation is 0.06 when the pulsation period and epoch of Petterson et al. (2004) are used. Hence, S Mus is much brighter than the quiescent phases. Thus the flux must be at least heavily dominated by the hot companion.

Appendix D
Systems with a Resolved Companion Closer than $2''$

In this appendix we discuss the components in systems with a resolved close companion. The results are summarized in Table 6.

S Nor: Although the companion is slightly closer than $1''$, the photometry in Table 4 from the WFC3 images is used. From an IUE spectrum, Evans (1992b) found a B9.5 V companion, which has essentially the same M_V as in Table 3, implying that it is the resolved companion.

Are there any other components in the system besides the Cepheid and the resolved component? An inner binary in the S Nor system is likely but not proven. Mermilliod et al. (1987) and Bersier et al. (1994) find little evidence of orbital motion in three well-covered seasons of CORAVEL data. Groenewegen (2008) found a low-amplitude orbit (2.53 km s^{-1}) with a period of 3584 days. However, the three seasons of CORAVEL data span 2700 days, so that orbital period seems unlikely (though not impossible). Gallenne et al. (2019) added radial-velocity data spanning 1700 days, but were unable to find an orbital signature. Kervella et al. (2019a) found differential proper motions between Hipparcos and Gaia marginally consistent with orbital motion. Combined with the orbit from Groenewegen, they found a companion mass of 1.5 $M_\odot$, approximately an F0 V star. The orbit has a semimajor axis of 8.87 au. Gallenne et al. (2019) observed the system with interferometry from the VLTI. If the hot star were the spectroscopic companion, it might have been marginally detectable, but they found no detection at a level greater than 2.3σ. An F0 V star would not be expected to be detected. (The resolved companion in Table 2 is outside the field.) In summary, this confirms that the resolved companion is probably the one dominating the IUE spectrum. Estimated properties of the inner binary are in Table 6. Thus, there is evidence of a short-period binary; however, an orbit is still uncertain, which may be due to a low-mass companion, the orbital inclination, or high eccentricity.

S Nor is a member of a cluster (NGC 6087), which may affect either the formation scenario or its dynamical history. One of the possible companions in our WFC3 survey is an

X-ray source (Paper IV; Table 6), with a separation from the Cepheid of 15″ or 13,300 au. The spectral type is derived from the $(V - I)_0$ color, using the calibration of Drilling & Landolt (2000). However, because it has an unusually large separation from the Cepheid (Figure 8), the conclusion in Paper IV was that it is likely to be a chance alignment with a cluster star, similar to the case of δ Cep. Kervella et al. (2019b) find additional companions at 41,100 and 38,800 au (Table 9), and note that many stars have similar proper-motion vectors. They do not confirm the companion discussed by Evans & Udalski (1994) at a separation of 32,000 au. The most likely companion properties for companions within 15″ are summarized in Table 6, although associated cluster members clearly complicate identification.

η *Aql*: Two companions to the Cepheid are known in this system. The companion in Table 5 is illustrated in Paper I and Figure 3. Gallenne et al. (2014a) used VLT/NACO to measure the properties of the companion at 0″.65, which they identify as an F1 V to F5 V star, corresponding to $(V - I)_0 = 0.37$–0.53 (Bessell & Brett 1988). They measure $H_0 = 9.34$. Using the calibration of Bessell and Brett, this corresponds to $V_0 = 10.1$–10.5. This is good agreement with a $V_0 = 10.0$ (Table 5), even at a separation of only 0″.6 from the Cepheid. At a distance of 273 pc, this corresponds to $M_V = +3.0$ to $+3.3$. In Tables 5 and 6 and Figures 6 and 7, we substitute the color $(V - I)_0 = 0.4$ and $M_V = +3.2$ for the contaminated color and magnitude in Table 2.

There is a second, hotter companion detected in an IUE spectrum, with a spectral type of B9.8 V (Evans 1991). In Table 6, V_0 and M_V are listed from that source. This second companion must be closer to the Cepheid and unresolved by either Gallenne et al. or in this study. However, neither it nor the Cepheid itself affect the measurement of companion in Table 4 using the resolved photometry of Gallenne et al. Unfortunately, Gaia data are poor for a star as bright as η Aql. Benedict et al. (2018) reported a preliminary orbit for the inner companion based on high-precision radial velocities of η Aql. Additional radial velocities (T. G. Barnes et al., 2020, in preparation) have not confirmed this orbit as yet. We include in Table 6 a very preliminary value of the semimajor axis estimated from the masses, and a period of 4 yr, which can at least be used in the schematic distribution of separations. While orbital information is sketchy, there is no doubt that there is a third star in the system, and that it is closer to the Cepheid than the resolved companion in Table 4. Preliminary indications are that the orbit is nearly face-on and possibly eccentric.

V659 Cen: As can be seen from the discovery image (Paper I, Figures 1 and 21), the companion in that image lies on a diffraction spike (in addition to being very close to the Cepheid), so the photometry is unreliable. However, there is information about the hottest companion from an IUE spectrum (Evans 1992b), in which the companion is found to be a B6.0 V star. This results in a corrected $E(B - V)$ for the Cepheid of 0.21 mag, and an absolute magnitude for the companion of -0.32 mag. A mild extrapolation from Table 15.11 of Drilling & Landolt (2000) provides $V - I = -0.16$.

The system was also resolved by Hipparcos (HIP 65970), with very similar parameters: PA 234°, separation 0″.574.

To search for a possible inner companion, radial velocities were investigated. The possible orbital motion for V659 Cen must be small, and Lloyd Evans (1968) rated it as questionable

at best. Lloyd Evans (1982) added new velocities to previous data, and concluded that the velocity differences between three seasons were probably not significant. However, R. I. Anderson (2020, in preparation) has identified orbital motion in a more recent series of observations. Kervella et al. (2019a) investigated Gaia DR2 and Hipparcos proper-motion anomalies as indications of orbital motion. They found marginal evidence in the Hipparcos data. The Gaia data show no significant anomaly, but the error in the proper-motion vector is unusually large, which could be due to orbital motion, particularly of a close companion. Based on this, we have added a tentative entry in Table 6 and Figure 8 of 3 au, reasonable for an orbit of a few years. Pending confirmation of orbital motion, V659 Cen would have both a resolved companion and a closer spectroscopic companion. Just prior to submission, we obtained an HST STIS G140L spectrum oriented to separate the resolved companion from the Cepheid. This spectrum shows that the resolved companion is the hottest star in the system, with the spectroscopic-binary companion being much cooler. Entries in Table 5 are based on the IUE spectral type. Kervella et al. (2019b) find an additional very wide (62″) gravitationally bound low-mass (M3 V) companion.

AX Cir: This is the closest companion to a Cepheid identified here, and has particular problems for that reason. It is clear from the F845M image, however, that there is a star partly obscured by the bleed column and a diffraction spike. For this reason, the F621M filter is not usable, hence a color is not available. In the discussion below, we use the results from an IUE spectrum for further information about the companion.

The AX Cir system has been resolved three times: 2018 (Tokovinin et al. 2019), 1991.25 (HIP 72773), and 1913 by Innes.

AX Cir is also a member of a binary system (Petterson et al. 2004). An IUE spectrum shows that the hottest star in the system is a B6 V star (Evans 1994). The system was resolved with VLTI/PIONIER interferometry (Gallenne et al. 2014b) with a projected separation of 29.2 ± 0.2 mas, which corresponds to a separation of 15.4 au at a distance of 527 pc. The separation of the wider companion (0″.3 in Table 4) corresponds to 158 au. An HST STIS spectrum (A. Gallenne et al., 2020 in preparation) showed that the B6 V star is the wider companion. From the STIS spectrum the spectral type of the close spectroscopic companion was found to be B9 V. A tentative velocity measure of the close companion from the STIS spectrum indicates that the most likely interpretation is that the inner companion is itself a short-period binary, making a total of four components in the system. Kervella et al. (2019a) find a strong indication from Gaia and Hipparcos proper motions of an anomaly, indicating a short-period orbit of the close companion. Combining this with the Petterson orbit and an estimated mass for the Cepheid, they find a companion mass higher than the Cepheid mass, confirming that the companion is itself a binary. Kervella et al. (2019b) also find a wider (81″.5 = 43000 au) likely gravitationally bound system member, which is a low-mass M3.5 V star (Table 9). As with V659 Cen, we include the M_V and $(V - I)_0$ inferred from the IUE spectrum in Table 6.

R Cru: There are three companion candidates to this system.

1. The M_V and $(V - I)_0$ in Table 5 correspond to an early K star. (The WFC3 photometry for a companion at this separation

is much less likely to have contamination from the Cepheid than closer companions.)

2. To check for additional system members, radial velocities were investigated as discussed above. The orbital motion in Figure 27 partly guided by the position of the X-ray source (Appendix C) provides evidence for a companion inside the one identified in this study (Table 3). Kervella et al. (2019b) also find find marginal evidence in Gaia and Hipparcos proper motions of short-period orbital motion, which would be consistent with the radial-velocity orbit. As a preliminary estimate of the separation for an inner companion, orbital motion within a year suggests a period of several years. We have used this approximation to add this companion to Figure 8 and Table 6. We know from IUE observations (Evans 1992a) that the companion in the system is cooler than A2, corresponding to a mass of 2.7 $M_\odot$.

3. We have also reinstated the 7″6 companion from Paper II for the following reasons. Kervella et al. (2019b) find that it is at the same distance as the Cepheid using Gaia data and is a gravitationally bound companion (spectral type G8 V). Possible orbital motion is detected. We note that there are X-ray counts from XMM in the position of that companion in Paper IV, although it is not the most prominent source in the field. The Chandra image (Figure 26) is a shallower image, hence this companion is not detected.

U Aql: In Appendix E we report extensive new material about U Aql, for which we provide a detailed discussion. There are three companions to the Cepheid in this system. M_V for the companions is from Table 13. The spectral type of the 1″6 companion is estimated to be A5 V from the STIS spectrum. We use the calibration of Drilling & Landolt (2000) of $(V - I)_0 = 0.16$. This is in agreement with the value in Table 11 for a companion with a separation of 1″6. Component B (close) has an estimated projected separation of 66 au and spectral type of A3–4 V (Appendix E).

The 1″6 pair of U Aql has been measured 12 times since the first resolution by Kuiper (1934). It has always been at about the same relative position.

The U Aql spectroscopic binary was resolved at three epochs with the VLTI PIONIER combination (Gallenne et al. 2019). Using a distance of 592 ± 19 pc, they determined preliminary masses for the Cepheid and the spectroscopic companion of 6.2 ± 0.8 and 2.2 ± 0.2 $M_\odot$, respectively. This is somewhat lower than the mass inferred from the B9.8 V spectral type using the Drilling & Landolt calibration. However, it agrees with the Harmanec (1988) calibration within the errors (decreased by 0.02 in log M because the companions of Cepheids will be younger than average main-sequence stars of their spectral type; Evans et al. 2018). A strong anomaly was detected in the Gaia and Hipparcos proper motions (Kervella et al. 2019a). The inferred separation and companion mass (assuming a Cepheid mass) are in agreement with those of Gallenne et al. (2019). The derived separation in Table 6 is the combined interferometric separation from Gallenne et al. and the distance from Paper II. No wider resolved companions were detected in the Gaia data (Kervella et al. 2019b).

U Vul: The M_V of the U Vul companion in Table 5 corresponds to a K0 star (Drilling & Landolt 2000). Another system member is indicated by an orbit for U Vul that was published by Imbert (1996), which has a high eccentricity and low amplitude. Kervella et al. (2019a) found a significant proper-motion anomaly in the Gaia and Hipparcos data.

Assuming a Cepheid mass, they found a mass for the spectroscopic companion of 2.4 ± 0.4 $M_\odot$ and a semimajor axis of 7.1 au. The upper limit of the spectral type from an IUE spectrum is A1 V, corresponding to a mass of 2.5 $M_\odot$, which is in agreement with (and very close to) the Kervella mass within the errors. Note that this upper limit pertains to any companion in the system, both the spectroscopic companion and the resolved companion (Table 4). No wider resolved companions were found in the Gaia DR2 data (Kervella et al. 2019b).

Appendix E
U Aql

The quest for masses and luminosities for Cepheid variables has benefited greatly from the availability of the ultraviolet spectrum using satellites (IUE and HST). Through these studies, the picture of multiplicity has become increasingly complex. U Aql = HD 183344 is a good case in point. Its substantial orbital motion was only recognized in 1979 (Slovak et al. 1979). Welch et al. (1987) provide an orbit, as well as a summary of previous velocity information. The spectrum of the hottest star in the system dominates in the ultraviolet below about 2000 Å, and IUE observations have been discussed by Böhm-Vitense & Proffitt (1985) and Evans (1992b). These provided a temperature of 9300 ± 100 K and a spectral type of B9.8 V, respectively.

E.1. Companions

New insight into the system came with HST Faint Object Camera (FOC) and Space Telescope Imaging Spectrograph (STIS) images (PI: D. Massa). The STIS image was made with the G230L grating and the STIS NUV-MAMA detector. A series of spectra were taken at varying roll angles and times in the orbit. Similar data are fully discussed for AW Per (Massa & Evans 2008) and W Sgr (Evans et al. 2009). One of the images is presented as an example in Figure 30. Unexpected complexity in the system is immediately evident. The spectroscopic binary is the bottom spectrum, with the Cepheid Aa as the brightest star in the long-wavelength region and the companion Ab as the brightest star in the short-wavelength region. At the top is the resolved companion C, found in the HST WFC3 imaging (Table 2). Between them, but very close to the spectroscopic binary, is a previously unsuspected companion B. The components are summarized in Table 6. In addition to the separation of C from Table 2, the projected separation of B has been measured from the STIS image. The separation in the spectroscopic binary Aa and Ab has been taken from the interferometry of Gallenne et al. (2019), 10.06 ± 0.16 mas. Using the distance from Paper II (613 pc), this becomes 6.2 au.

Companion B may be the interferometric pair resolved three times by Ismailov (1992). However, it was not resolved by speckle at SOAR in 2008 and 2016 (Tokovinin et al. 2010, 2018, respectively).

Spectra were extracted from the STIS image as described in Evans et al. (2009). The U Aql observations were made with the G230L and the unfiltered 25MAMA aperture. For the PSF comparison star we used the data set o6hr01040, an observation of the hot subdwarf GRW+70D5824. This exposure has a relatively high signal-to-noise ratio and was taken in 2002 February, only a few months before the first of the U Aql observations. The image of U Aql that was analyzed was o6f101020, selected because it has the best projected separation between the components. The projected separation
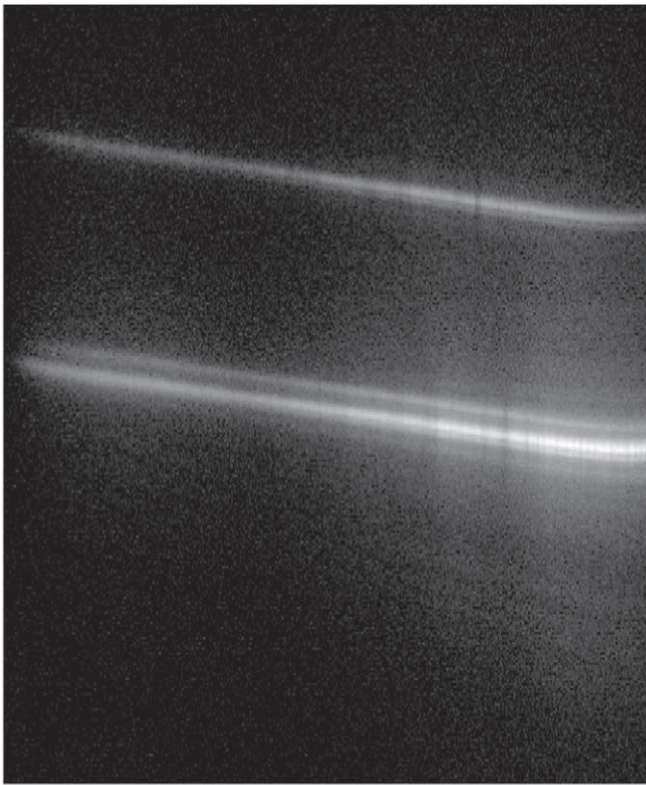
Figure 30. A flat-fielded image, o6f101020, of the U Aql system. The wavelength increases to the right from about 1796 to 3382 Å. The lower component has the Cepheid (Aa; brightest at long wavelengths) and also the hottest star in the system (Ab; brightest at short wavelengths). The component at the top (C) is the one identified in the HST imaging (Table 2). A third component (B) is between them, close to the spectroscopic binary containing the Cepheid. The spectrum is on a log scale. The strongest feature in the Cepheid spectrum is 2800 Å.
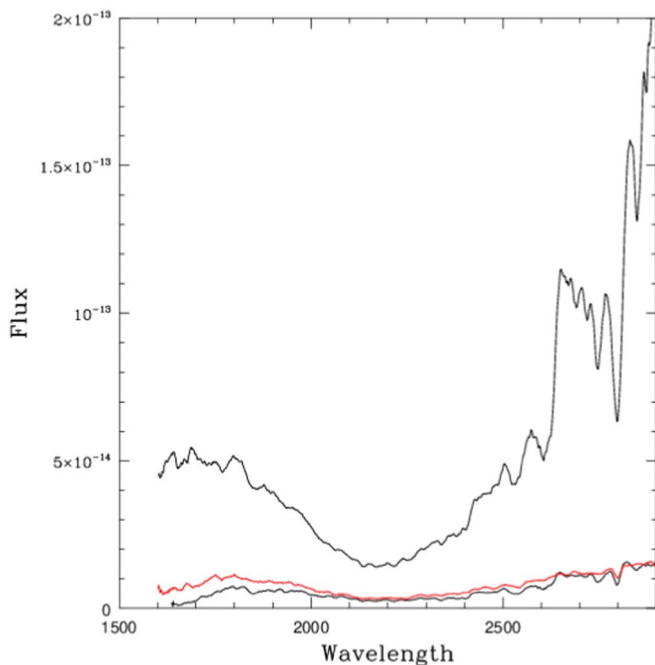
Figure 31. The extracted spectra for the U Aql system. The brightest spectrum is the spectroscopic binary containing the Cepheid and the hottest companion. The faintest spectrum is the wide companion. The spectrum in red is the close resolved companion.
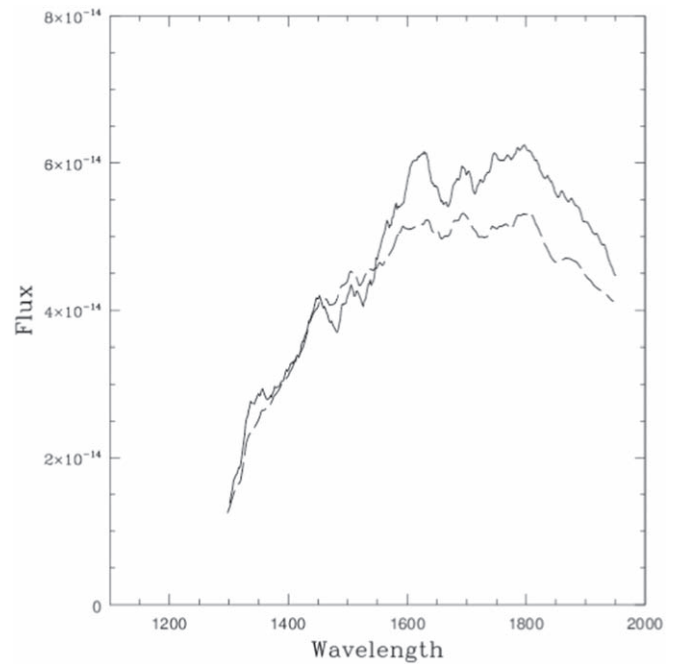

Figure 32. Comparison of the IUE spectra of U Aql and B9.8 V. The solid line is the U Aql spectrum, and the dashed line is the B9.8 V spectrum.

between the spectroscopic binary with the Cepheid and the closest companion is $0.''107$ using a plate scale of $0.''0247\,\mathrm{px}^{-1}$, which corresponds to 66 au using the distance from Paper II. The results are shown in Figure 31. The Cepheid dominates in the long-wavelength section, but the companions dominate at the short-wavelength end. Components B and C are resolved, and the Cepheid makes no contribution to the spectrum. For the spectroscopic binary Aa and Ab, however, in the region near 1800 Å there is still a contribution from the Cepheid, although the companion Ab dominates. In this section we estimate the spectral types of all three companions, and we correct for the contribution of the Cepheid to the spectrum of Ab as follows. We use the IUE spectra of standard stars to create a spectrum B9.8 V (midway between B9.5 V and A0 V) as in Evans (1992b). (The B9.8 V spectrum has been reddened to match the U Aql spectrum and then scaled for comparison.) Figure 32 shows that the B9.8 V spectrum represents the U Aql companion Aa well at wavelengths shorter than 1500 Å, but the additional contribution from the Cepheid can be seen at longer wavelengths. Therefore we use the flux from the B9.8 V spectrum to estimate the magnitude difference between the three companions in the U Aql system.

For all three companions in the U Aql system (Figure 33) the mean flux from 1650 to 1950 was created (Table 14), and from these, the magnitude difference between the companions and the U Aql spectrum was created. At the bottom of Table 14 the fluxes from the IUE spectra are given. From the difference between the B9.8 V spectrum and the composite U Aql spectrum (Aa + Ab at 1800 Å), a correction of 0.15 mag was derived to account for the contribution to the U Aql spectrum from the Cepheid. The far right column for the far (C) and close (B) companions from the STIS spectra includes this correction. Note that the IUE spectrum of the U Aql system includes all three companions, although the hottest star in the system (Ab) is only affected in a minor way at the shortest wavelengths.
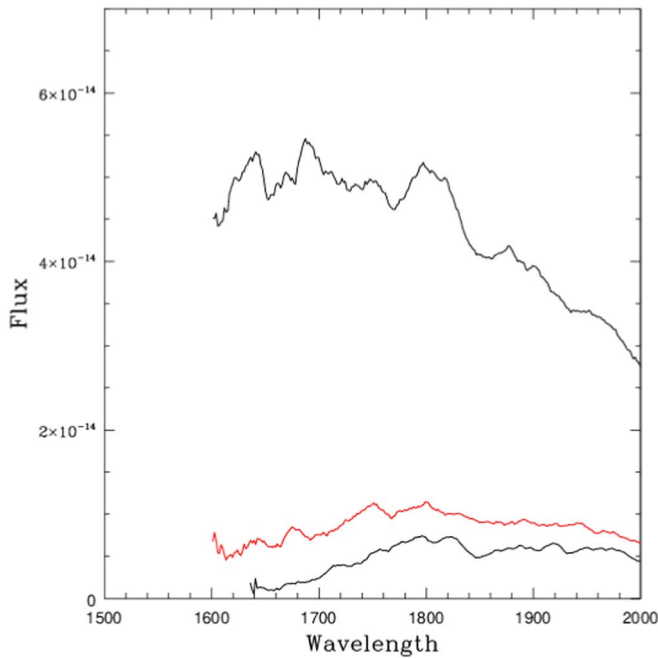
Figure 33. The three companions in the U Aql system in the short-wavelength region. As in Figure 31, the spectrum in red is from the close resolved companion (B). The spectroscopic binary is represented by the B9.8 V spectrum.
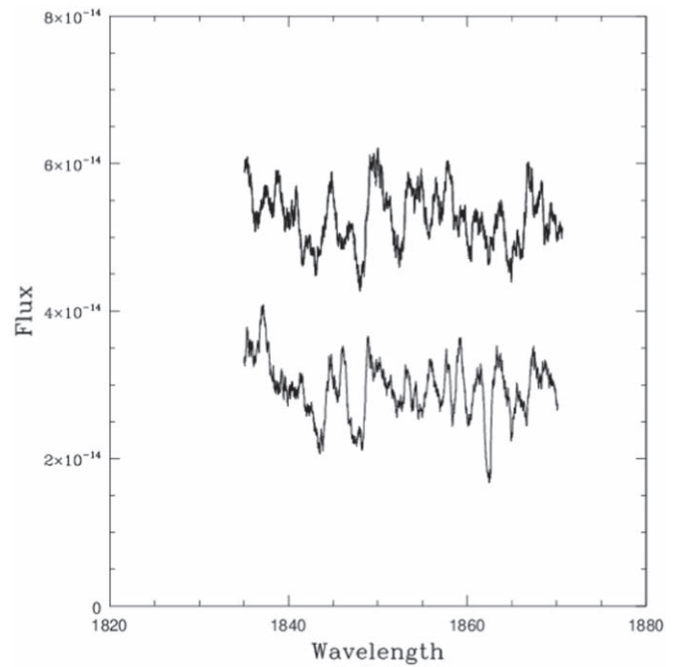

Figure 34. The spectral region used in this analysis. The bottom is the spectrum from day 1 (see text), and the top is the spectrum from day 2 shifted by 0.2×10^{-14} in flux for clarity. Both spectra have been smoothed by 100 points.

Table 13
Components of the U Aql System

ID	Sep. ″	Sep. (au)	M_V (mag)	SpTy
Ab	0.0101	6.2	1.2	B9.8 V
B	0.107	66	1.8	A3-4 V
C	1.6	981	2.1	A5 V

Table 14
Flux at 1800 Å

Star	$f(1800)$ erg cm^{-2} s^{-1} Å^{-1}	$\Delta M(1800)$ wrt U Aql	Corr.
	HST/STIS		
Far: C	5.01×10^{-15}	2.39	2.24
Close: B	9.14×10^{-15}	1.74	1.59
U Aql	4.52×10^{-14}		
	IUE		
U Aql	5.64×10^{-14}		
B9.8 V	4.89×10^{-14}		

The spectral type of companion Aa was derived in Evans (1992b). To estimate the spectral type of the magnitude differences (Table 14), Table 15 shows the magnitude differences for main sequence spectral types from the V—ultraviolet colors (Column 2) from Wesselius et al. (1980) and the absolute magnitude calibration (Column 3) from Drilling & Landolt (2000) for the ZAMS, which is essentially the same as used in Evans (1991, 1992b). The far component C is approximately A5 V, and the close component B is A3-4 V, corresponding to $M_V = +2.1$ and $+1.8$, respectively. This magnitude for C is very similar to that from the WFC3 value (Table 5).

E.2. Velocities

Previously, Evans et al. (1998) obtained spectra with the Goddard High Resolution Spectrograph (GHRS) to measure the orbital velocity amplitude of the spectroscopic-binary companion with the medium-resolution grating G200M. The velocity difference between the two is -29.1 km s^{-1} with an estimated error of 3.8 km s^{-1}. Combining this with the orbital velocity amplitude of the Cepheid (Welch et al. 1987) and the mass of the main sequence companion, they derived a mass for the Cepheid of 5.1 ± 0.7 $M_\odot$.

More recently, a spectrum was obtained with STIS. The spectrum used the E230H grating, and was taken over two days in 2003: August 1 (exposure time 12109 s), and 14 hr later on August 2 (exposure time 7375 s). When the orbit of Welch et al. (1987) is used, the orbital phase is 0.44. The data used are shown in Figure 34. A portion of the spectrum was selected where the blaze correction is satisfactory and there are spectral features. It was used in two ways. First the spectra for the two days were cross-correlated to look for a velocity difference that could be caused by motion in a short-period binary orbit. In addition, the STIS spectrum was cross-correlated with each of the GHRS spectra to confirm the orbital velocity amplitude in the 5 yr orbit.

Although the spectrum on each day was weak, the cross correlation of these two spectra provided the opportunity to check for possible orbital motion from a short-period binary. The spectral lines are reasonably broad, which is not surprising for a late-B main sequence star, resulting in a broad velocity peak. However, Figure 35 shows no evidence of a change in velocity, which would be an indication of short-term binary motion.

This is in agreement with the mass of the secondary in Kervella et al. (2019a) incorporating Gaia and Hipparcos
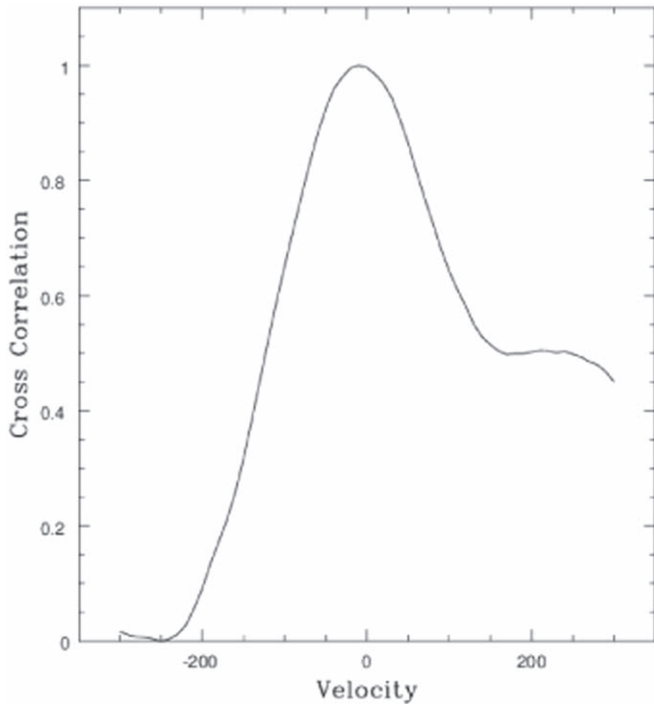
Figure 35. The cross correlation between the exposures on days 1 and 2.

Table 15
Energy Distributions of Companions

Spectral Type	$M(1800-V)$	M_V	$M(1800)$	$M-M$(B9.8)(1800)
B9 V	−0.90	+0.9	+0.0	⋯
B9.5 V	−0.70	+1.1	+0.4	⋯
B9.8 V	−0.60	+1.2	+0.6	⋯
A0 V	−0.51	+1.3	+0.8	0.2
A1 V	−0.21	+1.4	+1.2	0.6
A2 V	0.04	+1.5	+1.5	0.9
A3 V	0.27	+1.7	+2.0	1.4 B
A4 V	0.46	+1.9	+2.4	1.8 B
A5 V	0.68	+2.1	+2.8	2.2 C

proper motions with the orbit. The mass is appropriate for a B9.8 V star, and would not accommodate an additional star.

To check the result from the two GHRS spectra (Evans et al. 1998), the STIS spectrum was cross-correlated with each of the GHRS spectra. The result (Figure 36) showed a similar shift between the two orbital phases to that found previously. On the other hand, it is possible that the STIS spectrum is as much as 30 km s^{-1} smaller than both the GHRS spectra. In particular, the STIS spectrum should have a very similar orbital velocity to GHRS Visit 1.

In summary, the STIS spectra taken a day apart do not show any velocity signal that the companion is a very short-period binary. Comparison of the STIS and GHRS velocities (Figure 36) leaves open the possibility of a longer period binary with lower orbital velocity. However, because of the broad lines, and hence the broad correlation, this is only a possibility.

E.3. Discussion

The STIS image (Figure 30) provides an explanation for a surprisingly large discrepancy between an absolute magnitude
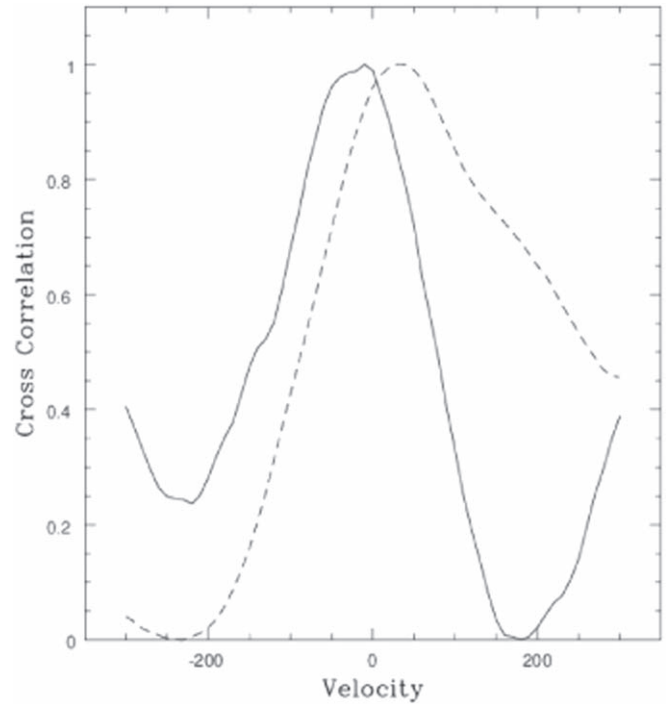

Figure 36. The cross correlation of the STIS spectrum with the two GHRS spectra. The solid line shows the velocity of the GHRS Visit 1 spectrum with respect to the STIS spectrum, and the dashed line plots GHRS Visit 2 with respect to STIS. The program returns velocities that are in the sense that the velocity of the companion has increased between Visits 1 and 2.

for the Cepheid from the IUE spectrum of the companion and the Leavitt law (period-luminosity relation) of Feast & Walker (1987). As discussed in Evans (1992b), typical differences between the IUE absolute magnitudes and those of Feast and Walker are 0.2 mag for well-exposed companion spectra with well-known reddening. For U Aql the difference was more than twice this value, even though both conditions were met. However, the addition of the flux from the two additional companions that were unknown at the time (but would have been in the IUE aperture) accounts for the discrepancy.

Appendix F
Companions in Systems with a Resolved Wide Companion (Wider than 2″)

In this appendix we discuss the components in systems with a resolved wide companion. The results are summarized in Table 7.

FF Aql: The interpretation of the companion in Table 4 from the ground has been challenging. Udalski & Evans (1993) concluded that it is not a physical companion. However, the WFC3 measures (Paper II) found the photometry consistent with a physical companion. The Washington Double Star Catalog (WDS) finds no relative motion between the companion and Cepheid, indicating that they are moving together. In the recent discussion of Gaia DR2 data, Kervella et al. (2019b) find that the parallax of the companion is consistent with that of the Cepheid, but that the proper motion has a projected relative velocity between the two of ≃30 km s^{-1}. However, they describe the position and parallax of the two stars as "quite remarkable from a statistical point of view," and suggest that binary motion in the companion is a possible explanation. FF Aql is a well-known spectroscopic binary.

Astrometric motion has been detected by Benedict et al. (2007). It has been tentatively resolved by CHARA MIRC (Gallenne et al. 2019), with a separation of 8.9 mas. It also has strong indication of orbital motion in Hipparcos–Gaia proper motions (Kervella et al. 2019a). Combining proper-motion information with the orbit, the separation (8.2 mas corresponding to 4.5 au) and mass of the companion ($0.8 \pm 0.1\,M_\odot$) were derived (Kervella et al. 2019a; in Table 7). This corresponds to a spectral type of approximately K0 V, which is later than the range estimated from IUE spectra (Evans et al. 1990). At present, the inferred masses from Benedict et al., Kervella et al., and Evans et al. are not consistent, but improvement from the next Gaia release should resolve this. Kervella et al. (2019b) do not find likely wider companions.

RV Sco: Hipparcos–Gaia proper motions clearly show orbital motion (Kervella et al. 2019a), as was suspected by Szabados (1989), identifying a spectroscopic binary. As a very preliminary estimate of the separation (for plotting purposes), we use estimated orbital period of 8000^d, corresponding to a semimajor axis of 14 au for reasonable masses. WDS measures for RV Sco indicate that the brighter resolved candidate at a separation of $6''0$ has no relative motion with the Cepheid, and hence is likely bound, making three components in the system. However, it is dynamically unlikely that both possible companions in Table 4 are bound, hence the $6''0$ is the most likely physical companion. An IUE observation of the system showed that all stars in the system are A3 V or later, corresponding to a mass of 1.9 $M_\odot$ or lower.

AP Sgr: Hipparcos–Gaia proper motions show a weak indication of orbital motion (Kervella et al. (2019a). Radial-velocity observations indicate possible low-amplitude orbital variation (Gieren 1982; Lloyd Evans 1982; Szabados 1989), with a period estimate of 7000 days. As with RV Sco, this has been used to derive a very preliminary estimate of the semimajor axis in Table 7. Additional velocity observations are needed to confirm this. This would continue the pattern of an interior orbit found in systems with resolved companions. Alternatively, the separation of the resolved companion is the second largest in Table 4, and the color of the companion is the reddest. This would be consistent with the companion being a line-of-sight coincidence with a field star. An IUE observation shows that any companion in the system is A5 V or later, corresponding to a mass of $\leqslant 1.8\,M_\odot$. Two wider possibly comoving candidates (49,000 and 28,200 au) have been identified by Kervella et al. (2019b). However, even the brightest (49,000 au) is cooler than even a late-M main sequence star. Both are fainter and cooler than the limit for our survey (hotter than M0 stars), so they are not included in Table 10.

BB Sgr: As with AP Sgr, there is some indication of low-level orbital velocity (Gieren 1982; Barnes et al. 1988; Szabados 1989), but it is not conclusive. Velocities are available from Gorynya et al. (1996, 1998) from 1994 to 1997. As discussed by Evans et al. (2015), they have a γ velocity of 6.6 km s^{-1}, which is very similar to velocities assembled in Szabados (1989). Furthermore, there is no orbital motion to within less than 1 km s^{-1} in the Gorynya et al. data. R. I. Anderson (2020, in preparation) also sees no orbital motion. Hipparcos–Gaia proper motions show no anomaly consistent with orbital motion (Kervella et al. 2019a). An IUE observation shows that any companion in the system is A0 V or later, corresponding to a mass of $\leqslant 2.1\,M_\odot$. BB Sgr is a

member of the open cluster Collinder 394 (Anderson et al. 2013). As with S Nor, this makes possible a line-of-sight coincidence with a cluster member, rather than a bound companion.

Y Car: Table 4 has two possible companions for Y Car, with similar separations from the Cepheid, but it is dynamically unlikely that both are bound companions. At larger separations, Kervella et al. (2019b) identify several stars with similar proper motions from Gaia, indicating that there may be a comoving group, making a chance line-of-sight alignment rather than a gravitationally bound companion likely for at least one of the candidates in Table 7. Y Car is a well-known spectroscopic binary (Petterson et al. 2004). A velocity from the HST STIS spectrum of the companion indicated that the companion is itself a binary (Evans et al. 2005). The spectral type and mass of the hottest star in the system was determined from an IUE spectrum to be B9.0 V and 2.4 $M_\odot$. Preliminary estimates of the inclination and mass of the companion using Hipparcos–Gaia proper motions (Kervella et al. 2019a) provide a total mass of the two companion stars of $2.8 \pm 0.4\,M_\odot$. (This is an estimate because the orbital period is relatively short, although there is a highly significant detection of orbital motion.) Because this is only slightly higher than the mass of the hotter star of the pair from the IUE spectrum, this implies that the second star in the companion pair has a low mass. The spectroscopic system with the Cepheid has been tentatively resolved (Gallenne et al. 2019) with VLTI PIONIER, with a separation of 2.5 mas, corresponding to 3.6 au. Table 7 summarizes the component properties considered most probable.

V350 Sgr: There is one possible resolved companion to V350 Sgr in Table 4. V350 Sgr is a well-known binary system, where the mass of the Cepheid has been measured (Evans et al. 2018). The mass of $5.2 \pm 0.3\,M_\odot$ comes from combining the ground-based orbit of the Cepheid with the orbital velocity amplitude of the companion from HST STIS spectra, and the mass of the companion inferred from IUE spectra of 2.5 $M_\odot$. The mass of the companion determined from the spectroscopic orbit and the Hipparcos–Gaia proper motions is approximately 2σ from this: $3.4 \pm 0.5\,M_\odot$ (Kervella et al. 2019b using the orbit derived by Gallenne et al. 2019). The proper motions have a strong orbital signature. A tentative resolution of the system was made with VLTI PIONIER (Gallenne et al. 2019) with a separation of 3.0 mas or 2.7 au. Outside the HST survey here, which includes $20''$ around the Cepheid, two candidate bound companions are found from proper-motion agreement (Kervella et al. 2019b), making it possible that the Cepheid is part of a four- or five-member system.

ORCID iDs

Nancy Remage Evans ⓘ https://orcid.org/0000-0002-4374-075X
H. Moritz Günther ⓘ https://orcid.org/0000-0003-4243-2840
Howard E. Bond ⓘ https://orcid.org/0000-0003-1377-7145
Gail H. Schaefer ⓘ https://orcid.org/0000-0001-5415-9189
Brian D. Mason ⓘ https://orcid.org/0000-0003-4824-0938
Margarita Karovska ⓘ https://orcid.org/0000-0003-1769-9201
Evan Tingle ⓘ https://orcid.org/0000-0001-9075-6167
Scott Wolk ⓘ https://orcid.org/0000-0002-0826-9261
Scott Engle ⓘ https://orcid.org/0000-0001-9296-3477
Edward Guinan ⓘ https://orcid.org/0000-0002-4263-2650
Ignazio Pillitteri ⓘ https://orcid.org/0000-0003-4948-6550

Charles Proffitt ● https://orcid.org/0000-0001-7617-5665
Pierre Kervella ● https://orcid.org/0000-0003-0626-1749
Alexandre Gallenne ● https://orcid.org/0000-0001-7853-4094
Richard I. Anderson ● https://orcid.org/0000-0001-
8089-4419

References

Anderson, R. I., Eyer, L., & Mowlavi, N. 2013, MNRAS, 434, 2238
Anderson, R. I., & Riess, A. G. 2018, ApJ, 861, 36
Barnes, T. G., Moffett, T. J., & Slovak, M. H. 1988, ApJS, 66, 43
Benedict, G. F., Barnes, T. G., Evans, N. R., et al. 2018, AAS Meeting, 231, 10905B
Benedict, G. F., McArthur, B. E., Feast, M., et al. 2007, AJ, 133, 1810
Bersier, D. 2002, ApJS, 140, 465
Bersier, D., Burki, G., Mayor, M., & Duquenoy, A. 1994, A&AS, 108, 25
Bessell, M. S. 1979, PASP, 91, 589
Bessell, M. S., & Brett, J. M. 1988, PASP, 100, 1134
Böhm-Vitense, E., & Proffitt, C. 1985, ApJ, 296, 175
Bradley, L., Sipőcz, B., Robitalle, T., et al. 2019, astropy/photutils: v0.7.2, Zenodo, doi:10.5281/zenodo.3568287
de Mink, D. E., Sana, H., Langer, N., Izzard, R. G., & Schneider, F. R. N. 2014, ApJ, 782, 7
Deacon, N. R., & Kraus, A. L. 2020, MNRAS, 496, 5176
Doe, S., Nguyen, D., Stawarz, C., et al. 2007, in ASP Conf. Series 376, Astronomical Data Analysis Software and Systems XVI, ed. R. A. Shaw et al. (San Francisco, CA: ASP), 543
Drilling, J. S., & Landolt, A. U. 2000, in Astrophysical Quantities, ed. A. N. Cox (New York: Springer), 381
Duchêne, G., & Kraus, A. 2013, ARA&A, 51, 269
Engle, S. G., Guinan, E. F., Harper, G. M., et al. 2017, ApJ, 838, 67
Evans, D. W., Riello, M., & DeAngeli, F. 2018, A&A, 616, A4
Evans, N. R. 1991, ApJ, 372, 597
Evans, N. R. 1992a, ApJ, 384, 220
Evans, N. R. 1992b, ApJ, 389, 657
Evans, N. R. 1994, ApJ, 436, 273
Evans, N. R., Berdnikov, L., Lauer, J., et al. 2015, AJ, 150, 13
Evans, N. R., Böhm-Vitense, E., Carpenter, K., Beck-Winchatz, B., & Robinson, R. 1998, ApJ, 494, 768
Evans, N. R., Bond, H. E., Schaefer, G. H., et al. 2013, AJ, 146, 93
Evans, N. R., Bond, H. E., Schaefer, G. H., et al. 2016a, AJ, 151, 129
Evans, N. R., Carpenter, K. G., Robinson, R., Kiezle, F., & Dekas, A. E. 2005, AJ, 130, 789
Evans, N. R., Massa, D., Fullerton, A., Sonneborn, G., & Iping, R. 2006, ApJ, 647, 1387
Evans, N. R., Massa, D., & Proffitt, C. 2009, AJ, 137, 3700
Evans, N. R., Pillitteri, I., Wolk, S., et al. 2016b, AJ, 151, 108
Evans, N. R., & Udalski, A. 1994, AJ, 108, 653
Evans, N. R., Welch, D. L., Scarfe, C. D., & Teays, T. J. 1990, AJ, 99, 1598
Feast, M. W., & Walker, A. R. 1987, ARA&A, 25, 345
Freeman, P. E., Doe, S., & Siemiginowska, A. 2001, in ASP Conf. Series 238, Astronomical Data Analysis Software and Systems X, ed. F. R. Harnden, Jr. et al. (San Francisco, CA: ASP), 483
Gaia Collaboration, Brown, A. G. A., Vallenari, A., et al. 2018, A&A, 616, A1
Gaia Collaboration, Prusti, T., de Bruijne, J. H. J., et al. 2016, A&A, 595, A1
Gallenne, A., Kervella, P., Borgniet, S., et al. 2019, A&A, 622, A164
Gallenne, A., Kervella, P., Merand, A., et al. 2014a, A&A, 567, A60
Gallenne, A., Mérand, A., Kervella, P., et al. 2014b, A&A, 561, L3
Gieren, W. 1982, ApJS, 49, 1
Gilliland, R., Rajan, A., & Deustua, S. 2010, Instrument Science Report WFC3 2010-10, Space Telescope Science Institute
Gorynya, N. A., Rastorguev, A. S., & Samus, N. N. 1996, AstL, 22, 175
Gorynya, N. A., Samus', N. N., Sachkov, M. E., et al. 1998, AstL, 24, 815
Groenewegen, M. A. T. 2008, A&A, 288, 25
Hack, W., Dencheva, N., & Fruchter, A. S. 2013, ASPC, 475, 49
Harmanec, P 1988, Bull Ast. Inst Czech, 39, 329
Harnden, F. R., Branduardi, G., Elvis, M., et al. 1979, ApJL, 234, L51
Imbert, M. 1996, A&AS, 116, 497
Ismailov, R. M. 1992, A&AS, 96, 375
Kervella, P., Gallenne, A., Evans, N. R., et al. 2019a, A&A, 623, A116
Kervella, P., Gallenne, A., Evans, N. R., et al. 2019b, A&A, 623, A117
Kroupa, P. 1995, MNRAS, 227, 1491
Kuiper, G. 1934, PASP, 46, 188
Lafrenière, D., Marois, C., Doyon, R., et al. 2007, ApJ, 660, 770
Lloyd Evans, T. 1968, MNRAS, 141, 109
Lloyd Evans, T. 1982, MNRAS, 199, 925
Marois, C., Correia, C., Galicher, R., et al. 2014, Proc. SPIE, 9148, 91480U
Massa, D., & Evans, N. R. 2008, MNRAS, 383, 139
Mermilliod, J. C., Mayor, M., & Burki, G. 1987, A&AS, 70, 389
Moe, M., & Di Stefano, R. 2017, ApJS, 230, 15
Moe, M., & Kratter, K. M. 2018, ApJ, 854, 44
Naoz, S. 2016, ARA&A, 54, 411
Pecaut, M. J., & Mamajek, E. E. 2013, ApJS, 208, 9
Petterson, O. L., Cottrell, P. L., & Albrow, M. D. 2004, MNRAS, 350, 95
Reipurth, B., & Mikkola, S. 2012, Natur, 492, 221
Sana, H. 2017, in IAU Symp. 329, The Lives and Death-Throes of Massive Stars, ed. J. J. Eldridge et al. (Cambridge: Cambridge Univ. Press), 110
Sana, H., de Mink, S. E., de Koter, A., et al. 2012, Sci, 337, 444
Sana, H., LeBouquin, J.-B., & Lacour, S. 2014, ApJS, 215, 15
Slovak, M. H., Van Citters, G. W., & Barnes, T. G. 1979, PASP, 91, 840
Soummer, R., Pueyo, L., & Larkin, J. 2012, ApJ, 755, 28S
Stetson, P. 1987, PASP, 99, 191S
Szabados, L. 1989, CoKon, 94, 1
Szabados, L., Anderson, R. I., Derekas, A., et al. 2013, MNRAS, 434, 870
The Astropy Collaboration 2013, A&A, 558, 33A
Tody, D. 1986, Proc. SPIE, 627, 733
Tody, D. 1993, in ASP Conf. Series 52, Astronomical Data Analysis Software and Systems II, ed. R. J. Hanisch et al. (San Francisco, CA: ASP), 173
Tokovinin, A. 2017, MNRAS, 468, 3461
Tokovinin, A. 2018a, AJ, 155, 160
Tokovinin, A. 2018b, ApJS, 235, 6
Tokovinin, A., Mason, B. D., & Hartkopf, W. I. 2010, AJ, 139, 743
Tokovinin, A., Mason, B. D., & Hartkopf, W. I. 2018, AJ, 155, 235
Tokovinin, A, Mason, B. D., Mendez, R. A., et al. 2019, AJ, 158, 48
Torres, G., Andersen, J., & Gimenez, A. 2010, A&ARv, 18, 67
Udalski, A., & Evans, N. R. 1993, AJ, 106, 348
Usenko, I. A., Kniazev, A. Y., Berdnikov, L. N., Fokin, A. B., & Kravtsov, V. V. 2014, AstL, 40, 435
Wahhaj, Z., Cieza, L., Mawet, D., et al. 2015, A&A, 581, A24
Welch, D. L., Evans, N. R., Lyons, R. W., et al. 1987, PASP, 99, 610
Wesselius, P. R., van Duinen Aalders, J. W. G., & Kester, D. 1980, A&A, 85, 221